Reduced Order Modeling For The Nonlinear Geometric Response Of A Curved Beam

by

Yao-Wen Chang

A Thesis Presented in Partial Fulfillment
of the Requirements for the Degree
Master of Science

Approved July 2011 by the
Graduate Supervisory Committee:

Marc Mignolet, Chair
Joseph Davidson
Stephen Spottswood

ARIZONA STATE UNIVERSITY

August 2011

ABSTRACT

The focus of this investigation is on the renewed assessment of nonlinear reduced order models (ROM) for the accurate prediction of the geometrically nonlinear response of a curved beam. In light of difficulties encountered in an earlier modeling effort, the various steps involved in the construction of the reduced order model are carefully reassessed. The selection of the basis functions is first addressed by comparison with the results of proper orthogonal decomposition (POD) analysis. The normal basis functions suggested earlier, i.e. the transverse linear modes of the corresponding flat beam, are shown in fact to be very close to the POD eigenvectors of the normal displacements and thus retained in the present effort. A strong connection is similarly established between the POD eigenvectors of the tangential displacements and the dual modes which are accordingly selected to complement the normal basis functions.

The identification of the parameters of the reduced order model is revisited next and it is observed that the standard approach for their identification does not capture well the occurrence of snap-throughs. On this basis, a revised approach is proposed which is assessed first on the static, symmetric response of the beam to a uniform load. A very good to excellent matching between full finite element and ROM predicted responses validates the new identification procedure and motivates its application to the dynamic response of the beam which exhibits both symmetric and antisymmetric motions. While not quite as accurate as in the static case, the reduced order model predictions match well their full Nastran counterparts and support the reduced order model development strategy.

DEDICATION

To my parents, my twin brother, and my sister.

ACKNOWLEDGMENTS

I would like to thank my advisor, Dr. Mignolet, for all his guidance; support and the opportunity. Thanks to Dr. Davidson for his teaching and participation in my committee and to Dr. Spottswood for being one of my committee member and his time and effort in traveling to the defense. I would also like to acknowledge Dr. Wang, who has given me so much help and instruction.

TABLE OF CONTENTS

Page

LIST OF TABLES

LIST OF FIGURES

Chapter 1

INTRODUCTION

Modal models have long been recognized as the computationally efficient analysis method of complex linear structural dynamic systems, yielding a large reduction in computational cost but also allowing a convenient coupling with other physics code, e.g. with aerodynamics/CFD codes for aeroelastic analyses. Further, these modal models are easily derived from a finite element model of the structure considered and thus can be obtained even for complex geometries and boundary conditions. However, a growing number of applications require the consideration of geometric nonlinearity owing to the large structural displacements. For example, panels of supersonic/hypersonic vehicles have often in the past been treated in this manner because of the large acoustic loading they are subjected to as well as possible thermal effects. Novel, very flexible air vehicles have provided another, more recent class of situations in which geometric nonlinearity must be included.

For such problems, it would be very desirable to have the equivalent of the modal methods exhibiting: (i) high computational efficiency, (ii) an ease of coupling to other physics codes, and (iii) generality with respect to the structure considered and its boundary conditions. To this end, nonlinear reduced order modeling techniques have been proposed and validated in the last decade [1-13]. Although several variants exist, their construction share the same aspects. First, they involve a *parametric* form of the model, i.e. one in which the nonlinearity is only on the “stiffness” and includes linear, quadratic, and cubic terms of the

displacement field generalized coordinates (see chapter below). Second, they rely on an identification strategy of the parameters of the model, i.e. the linear, quadratic, and cubic stiffness coefficients, from a finite element model of the structure for a particular set of “modes” or basis functions. Differences between the existing methods center in particular on the way the linear and nonlinear stiffness coefficients are estimated from a finite element model and on the extent and specificity of the basis functions, i.e. modeling of only the displacements transverse to the structure or all of them.

As may be expected, the first validations of these reduced order models focused on flat structures, beams and plates, and an excellent match between responses predicted by the reduced order models and their full finite element counterparts have been demonstrated. Curved structures, curved beam most notably, have also been investigated in the last few years and a very good match of reduced order model and full finite element results was obtained. Yet, the construction of the reduced order model was not as straightforward in this case as it had been in flat structure, instabilities of the model were sometime obtained.

The issue of constructing stable and accurate nonlinear reduced order models for curved structures is revisited here and an extension of the displacement-based (STEP) identification procedure [14, 8] is first proposed. Then, its application to a curved beam model is demonstrated, and shown to lead to an excellent matching between reduced order model and full finite element predictions.

Chapter 2

PARAMETRIC FORMS OF NONLINEAR REDUCED ORDER MODELS

The reduced order models considered here are representations of the response of elastic geometrically nonlinear structures in the form

$$\hat{u}_i(\underline{X},t) = \sum_{n=1}^{M} q_n(t)\,\hat{\psi}_i^{(n)}(\underline{X}) \ , \ i = 1, 2, 3 \qquad (2.1)$$

where $\hat{u}_i(\underline{X},t)$ denotes the displacement components at a point $\underline{X} = (X_1, X_2, X_3)$, see Fig. 2.1, of the structure and at time *t*. Further, $\hat{\psi}_i^{(n)}(\underline{X})$ are specified, constant basis functions and $q_n(t)$ are the time dependent generalized coordinates.

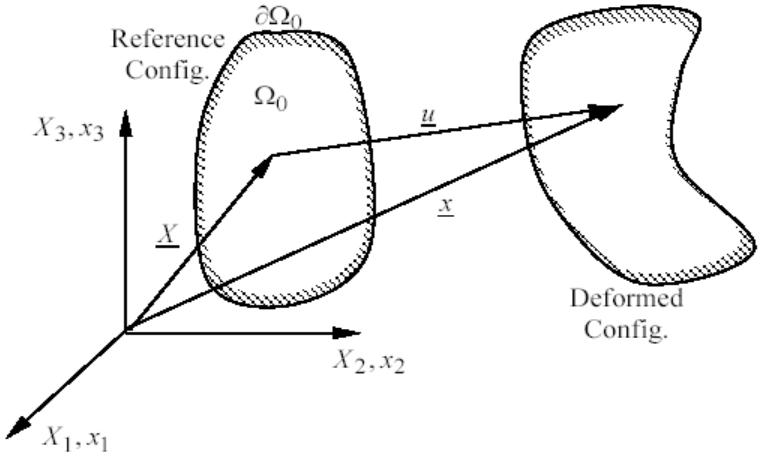

Figure 2.1. Reference and deformed configurations [16].

A general derivation of linear modal models is classically carried out from linear (infinitesimal) elasticity and it is thus desired here to proceed similarly but with finite deformation elasticity to include the full nonlinear geometric effects. Then, the first issue to be addressed is in what configuration, deformed or undeformed, the governing equations ought to be written. In this regard, note that

the basis functions $\hat{\psi}_i^{(n)}(\underline{X})$ are expected to (a) be independent of time and (b) satisfy the boundary conditions (at least the geometric or Dirichlet ones). These two conditions are not compatible if the basis functions are expressed in the deformed configuration as the locations at which the boundaries are will vary with the level of deformations or implicitly with time. However, these conditions are compatible if one proceeds in the undeformed configuration and thus $\underline{X}$ in Eq. (2.1), will denote the coordinates of a point in the undeformed configuration.

Accordingly, the equations of motion of an infinitesimal element can be expressed as (e.g. see [15, 16], summation over repeated indices assumed)

$$\frac{\partial}{\partial X_k}\left(F_{ij}\, S_{jk}\right) + \rho_0\, b_i^0 = \rho_0\, \ddot{\hat{u}}_i \text{ for } \underline{X} \in \Omega_0 \qquad (2.2)$$

where S denotes the second Piola-Kirchhoff stress tensor, ρ_0 is the density in the reference configuration, and $\underline{b}^0$ is the vector of body forces, all of which are assumed to depend on the coordinates X_i. Further, in Eq. (2.2), the deformation gradient tensor F is defined by its components F_{ij} as

$$F_{ij} = \frac{\partial x_i}{\partial X_j} = \delta_{ij} + \frac{\partial \hat{u}_i}{\partial X_j} \qquad (2.3)$$

where δ_{ij} denotes the Kronecker symbol and the displacement vector is $\hat{u} = \underline{x} - \underline{X}$, $\underline{x}$ being the position vector in the deformed configuration. Finally, Ω_0 denotes the domain occupied by the structure in the undeformed configuration. It has a boundary $\partial\Omega_0$ composed of two parts: $\partial\Omega_0^t$ on which the tractions $\underline{t}^0$ are given

and $\partial\Omega_0^u$ on which the displacements are specified (assumed zero here). Thus, the boundary conditions associated to Eq. (2.2) are

$$F_{ij}\, S_{jk}\, n_k^0 = t_i^0 \quad \text{for } \underline{X} \in \partial\Omega_0^t \tag{2.4}$$

$$\hat{u} = \underline{0} \quad \text{for } \underline{X} \in \partial\Omega_0^u \tag{2.5}$$

Note in Eqs (2.2) and (2.4) that the vectors $\underline{b}^0$ and $\underline{t}^0$ correspond to the transport ("pull back") of the body forces and tractions applied on the deformed configuration, i.e. $\underline{b}$ and $\underline{t}$, back to the reference configuration (see [15, 16]).

To complete the formulation of the elastodynamic problem, it remains to specify the constitutive behavior of the material. In this regard, it will be assumed here that the second Piola-Kirchhoff stress tensor *S* is linearly related to the Green strain tensor *E* defined as

$$E_{ij} = \frac{1}{2}\left(F_{ki}\, F_{kj} - \delta_{ij}\right) \tag{2.6}$$

That is,

$$S_{ij} = C_{ijkl}\, E_{kl} \tag{2.7}$$

where C_{ijkl} denotes the fourth order elasticity tensor.

Introducing the assumed displacement field of Eq. (2.1) in Eqs (2.2)-(2.7) and proceeding with a Galerkin approach leads, after some manipulations, to the desired governing equations, i.e.

$$M_{ij}\ddot{q}_j + D_{ij}\dot{q}_j + K_{ij}^{(1)}\, q_j + K_{ijl}^{(2)} q_j q_l + K_{ijlp}^{(3)} q_j q_l q_p = F_i \tag{2.8}$$

in which M_{ij} are mass components, $K_{ij}^{(1)}$, $K_{ijl}^{(2)}$, and $K_{ijlp}^{(3)}$ are the linear, quadratic, and cubic stiffness coefficients, and F_i are the modal forces. Note that the damping term $D_{ij}\,\dot{q}_j$ has been added in Eq. (2.8) to collectively represent various dissipation mechanisms. Further, the symmetrical role of j and l in the quadratic terms and j, l, and p in the cubic ones indicates that the summations over those indices can be restricted to $p \geq l \geq j$.

Once the generalized coordinates $q_j(t)$ have been determined from Eq. (2.8), the stress field can also be evaluated from Eqs. (2.3), (2.6), and (2.7). Specifically, it is found that every component of the second Piola-Kirchhoff stress tensor can be expressed as

$$S_{ij} = \overline{S}_{ij} + \sum_{m} \hat{S}_{ij}^{(m)} q_m + \sum_{m,n} \tilde{S}_{ij}^{(m,n)} q_m\, q_n \tag{2.9}$$

where the coefficients $\overline{S}_{ij}$, $\hat{S}_{ij}^{(m)}$, and $\tilde{S}_{ij}^{(m,n)}$ depend only on the point $\underline{X}$ considered.

The governing equations for the full finite element model can be derived as in Eqs (2.1)-(2.8) but with the coordinates q_i replaced by the finite element degrees of freedom u_i and the basis functions $\hat{\psi}_i^{(n)}(\underline{X})$ becoming the element interpolation functions. This process accordingly leads to the equations

$$\hat{M}_{ij} u_j + \hat{D}_{ij} \dot{u}_j + \hat{K}_{ij}^{(1)} u_j + \hat{K}_{ijl}^{(2)} u_j u_l + \hat{K}_{ijlp}^{(3)} u_j u_l u_p = \hat{F}_i \tag{2.10}$$

Introducing in Eq. (2.10) a modal expansion of the form of Eq. (2.1), i.e.

$$\underline{u}(t) = \sum_{n=1}^{M} q_n(t)\, \underline{\psi}^{(n)} \tag{2.11}$$

where $\underline{\psi}^{(n)}$ are basis functions and $q_n(t)$ are the associated generalized coordinates recovers Eq. (2.8) and Eq. (2.9) as expected.

Chapter 3

INDENTIFICATION OF THE REDUCED ORDER MODEL PARAMETERS

One of the key component of the present as well as related nonlinear reduced order modeling approaches (see introduction) is the identification of the parameters of Eqs (2.8) and (2.9) from a finite element model of the structure considered in a standard (e.g. Nastran, Abaqus, Ansys) software. The reliance on such commercial codes gives access to a broad database of elements, boundary conditions, numerical algorithms, etc. but is a challenge from the standpoint of the determination of the parameters of Eqs (2.8) and (2.9) as one has only limited access to the detailed element information and matrices.

The estimation of the mass components M_{ij} and modal forces F_i is achieved as in linear modal models, i.e.

$$M_{ij} = \underline{\psi}^{(i)T} M_{FE} \underline{\psi}^{(j)} \tag{3.1}$$

$$F_i = \underline{\psi}^{(i)T} \underline{F}(t) \tag{3.2}$$

where M_{FE} is the finite element mass matrix and $\underline{F}(t)$ is the excitation vector on the structure.

Next is the determination of the stiffness coefficients $K_{ij}^{(1)}$, $K_{ijl}^{(2)}$, and $K_{ijlp}^{(3)}$. In this regard, note first that the linear coefficients $K_{ij}^{(1)}$ could be determined as in linear modal models, i.e.

$$K_{ij}^{(1)} = \underline{\psi}^{(i)T} K_{FE}^{(1)} \underline{\psi}^{(j)} \tag{3.3}$$

where $K_{FE}^{(1)}$ is the finite element linear stiffness matrix. Another approach must be adopted however for $K_{ijl}^{(2)}$ and $K_{ijlp}^{(3)}$ as nonlinear stiffness matrices are typically not available. Two approaches have been proposed to identify these parameters (and potentially the linear ones as well) from a series of static finite element solutions. The first one relies on prescribing a series of load cases and projecting the induced responses on the basis functions $\underline{\psi}^{(n)}$ to obtain the corresponding generalized coordinates values $q_j^{(p)}$, p being the index of the load cases. Then, introducing these values into Eq. (2.8) for each load case yields

$$K_{ij}^{(1)} q_j^{(p)} + K_{ijl}^{(2)} q_j^{(p)} q_l^{(p)} + K_{ijlr}^{(3)} q_j^{(p)} q_l^{(p)} q_r^{(p)} = F_i^{(p)} \qquad i = 1, ..., M \tag{3.4}$$

Proceeding similarly for P load cases yields a set of linear algebraic equations for the coefficients $K_{ijl}^{(2)}$ and $K_{ijlp}^{(3)}$, and possibly the linear stiffness coefficients $K_{ij}^{(1)}$ as well, which can be solved in a least squares format to complete the identification of the stiffness parameters.

An alternate strategy has also been proposed (e.g. see [14]) in which the *displacements* are prescribed and the required force distributions are obtained from the finite element code. The corresponding modal forces are then evaluated from Eq. (3.3) and a set of equations of the form of Eq. (3.5) is again obtained. Appropriately selecting the displacement fields to be imposed can lead to a

particularly convenient identification of the stiffness coefficients. Specifically, the imposition of displacements proportional to the basis function $\underline{\psi}^{(n)}$ only, i.e.

$$\begin{aligned} \underline{u} &= q_n \ \underline{\psi}^{(n)} \\ \hat{\underline{u}} &= \hat{q}_n \ \underline{\psi}^{(n)} \\ \tilde{\underline{u}} &= \tilde{q}_n \ \underline{\psi}^{(n)} \end{aligned} \tag{3.5}$$

leads to the 3 sets of equations

$$\begin{aligned} K_{in}^{(1)} \ q_n + K_{inn}^{(2)} q_n^2 + K_{innn}^{(3)} \ q_n^3 &= F_i \\ K_{in}^{(1)} \ \hat{q}_n + K_{inn}^{(2)} \hat{q}_n^2 + K_{innn}^{(3)} \ \hat{q}_n^3 &= \hat{F}_i \\ K_{in}^{(1)} \ \tilde{q}_n + K_{inn}^{(2)} \tilde{q}_n^2 + K_{innn}^{(3)} \ \tilde{q}_n^3 &= \tilde{F}_i \end{aligned} \tag{3.6}$$

(no sum on n)

for $i = 1, ..., M$. In fact, these 3 sets of equations permit the direct evaluation of the coefficients $K_{in}^{(1)}$, $K_{inn}^{(2)}$, and $K_{innn}^{(3)}$ for all i. Repeating this effort for $n = 1, ..., M$ thus yields a first set of stiffness coefficients.

Proceeding similarly but with combinations of two basis functions, i.e.

$$\underline{u} = q_n \ \underline{\psi}^{(n)} + q_m \ \underline{\psi}^{(m)} \quad m \geq n \tag{3.7}$$

and relying on the availability of the coefficients $K_{in}^{(1)}$, $K_{inn}^{(2)}$, $K_{innn}^{(3)}$ and $K_{im}^{(1)}$, $K_{imm}^{(2)}$, $K_{immm}^{(3)}$ determined above, leads to equations involving the three coefficients $K_{inm}^{(2)}$, $K_{innm}^{(3)}$, and $K_{inmm}^{(3)}$. Thus, imposing three sets of

displacements of the form of Eq. (3.8) provides the equations needed to also identify $K^{(2)}_{inm}$, $K^{(3)}_{innm}$, and $K^{(3)}_{inmm}$.

Finally, imposing displacement fields linear combination of three modes, i.e.

$$\underline{u} = q_n \ \underline{\psi}^{(n)} + q_m \ \underline{\psi}^{(m)} + q_r \ \underline{\psi}^{(r)} \qquad r \geq m \geq n \tag{3.8}$$

permits the identification of the last coefficients, i.e. $K^{(3)}_{inmr}$.

The above approach, referred to as the STEP (STiffness Evaluation Procedure), has often been used and has generally led to the reliable identification of the reduced order model parameters, especially in connection with flat structures, with values of the generalized coordinates q_n of the order of, or smaller than, the thickness. However, in some curved structures, e.g. the curved beam of [11], models identified by the STEP process are sometimes found to be unstable, i.e. a finite valued static solution could not be obtained with a time marching algorithm, when the applied load magnitude exceeded a certain threshold. This problem occurred most notably for loads inducing a snap-through of the curved beam. On other occasions, the matching obtained was poor although the basis appeared sufficient (see section 4.2 for discussion of this issue) for an accurate representation.

Such a situation is shown in Fig. 3.2 for the curved beam of Fig. 3.1 with the ROM of [11]. The model identified as above was indeed unstable when loaded to a static force of P = 3 lb/in. This issue led in [11] to an ad hoc zeroing out of some of the coefficients of the model leading to the predictions shown in Fig. 3.2.

These results match quite well their Nastran counterparts but such an effort is not easily repeated to any other structure for which the terms to be zeroed out are not easily predicted.

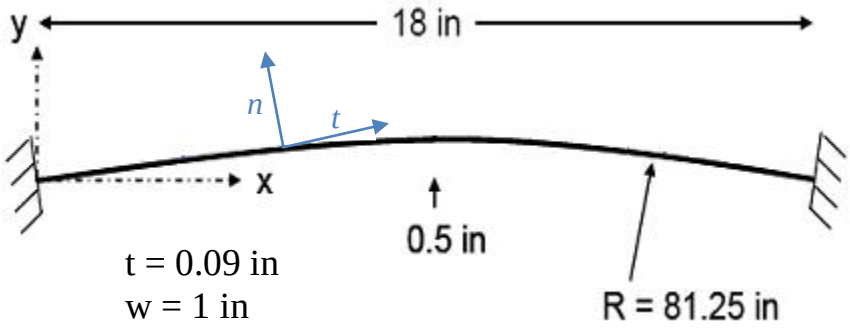

Figure 3.1. Curved beam geometry.

It was conjectured from [11] that the difficulty in capturing a stable snap-through response is due to the lack of continuity in the corresponding displacement vs. load curve. To assess better the difficulties, the snap-through Nastran displacement field corresponding to the uniform load P = 2 lb/in was scaled through a broad range of amplitudes. Each such displacement field was imposed in Nastran and the forces necessary to achieve it were determined. Projecting these forces on the scaled displacement provided the “modal force” required.

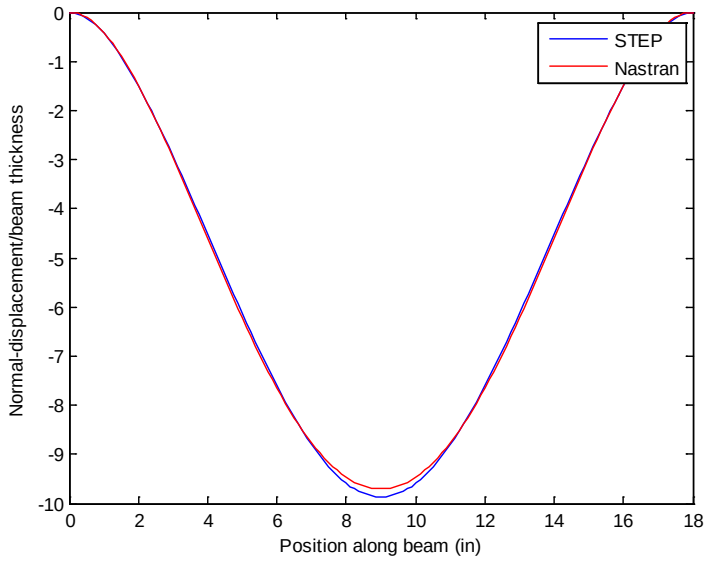

(a)

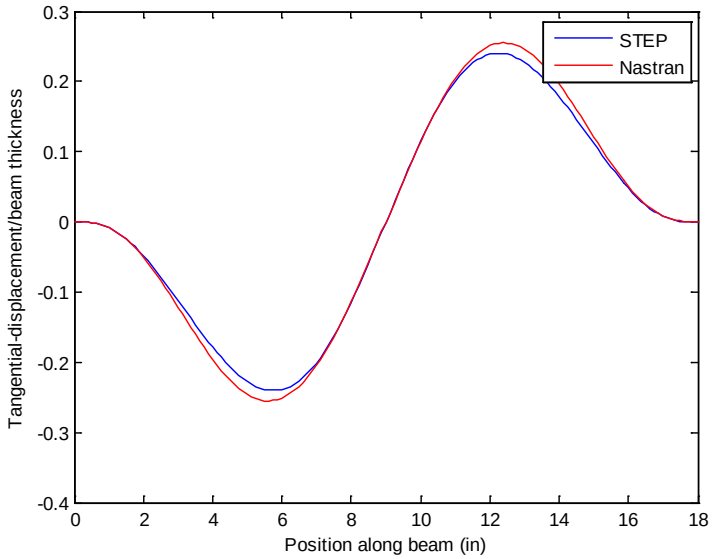

(b)

Figure 3.2. Comparison of static responses predicted by Nastran and by the reduced order model, curved beam, P = 2 lb/in.

(a) Normal and (b) tangential displacements.

Then, shown in Fig. 3.3, curve labeled Nastran, is the obtained modal force vs. modal displacement (i.e. the scaling of the Nastran displacement of Fig. 3.2) curve. The mass normalized P = 2 lb/in displacement was then used as a single mode and the STEP identification was performed to get the corresponding linear, quadratic, and cubic coefficients for various values of the parameter q_1 of Eq. (3.5). The corresponding modal force vs. modal displacement curves are also shown in Fig. 3.3. Differences clearly occur between the Nastran and STEP curves, either at low or high displacement levels. A similar process was repeated with the 12-mode model of [11] before the zeroing out operation and the comparison with the Nastran results is shown in Fig. 3.4 which shows larger differences than in Fig. 3.3. This observation suggests that the identification of an accurate model becomes more challenging as the number of modes increases.

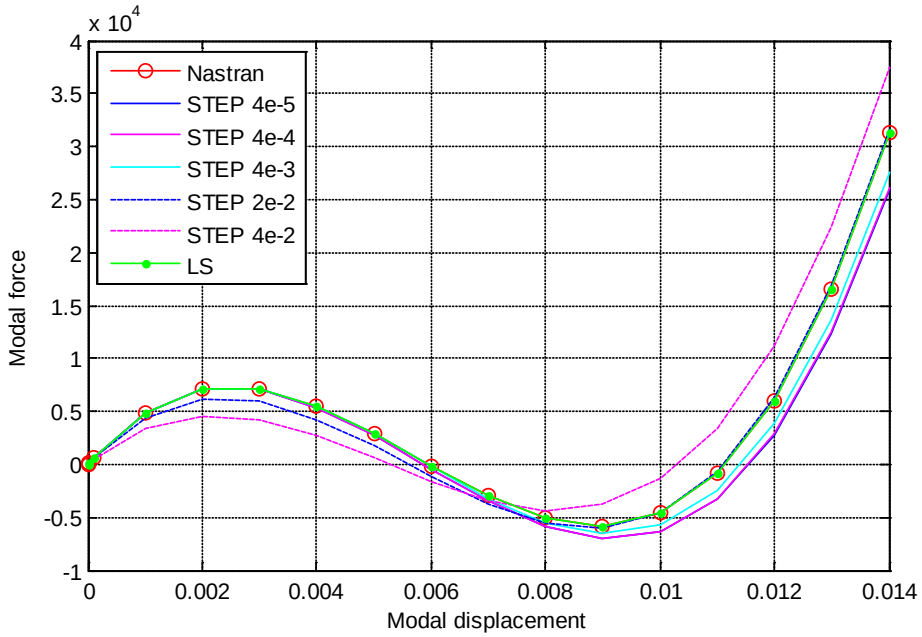

Figure 3.3. Modal forces versus modal displacements curves of 1-mode models identified by STEP and LS.

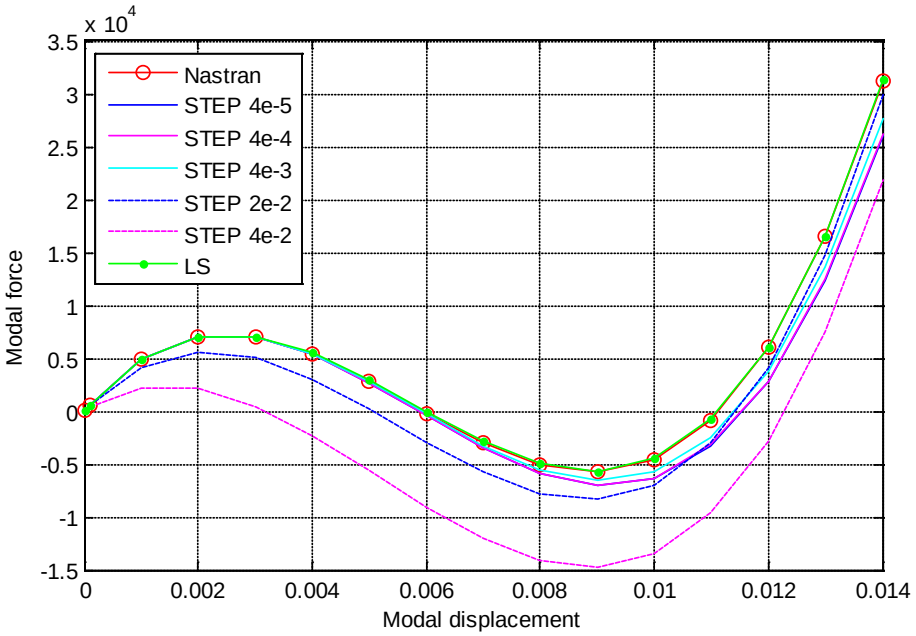

Figure 3.4. Modal forces versus modal displacements curves of 12-mode models identified by STEP and LS.

Table 3.1. Lowest eigenvalue of the matrix $\mathbf{K}_B$ for different STEP identified models and a LS identified model.

	q1	1 mode	12 modes
STEP	4.00E-05	2.17E+04	2.21E+04
STEP	4.00E-04	2.52E+04	2.39E+04
STEP	4.00E-03	7.06E+04	6.48E+04
STEP	2.00E-02	1.77E+04	-2.54E+05
STEP	4.00E-02	2.43E+04	-1.20E+06
LS	4.00E-04	1.31E+05	1.42E+05

The lack of a close matching in Fig. 3.3 and 3.4 of the STEP results with their Nastran counterpart suggests that neither the 1-mode nor the 12-mode model would provide a close fit of the displacements on Fig. 3.2 but does not seem to justify the instability observed. A different perspective on this issue can be obtained by analyzing the eigenvalues of the matrix $\mathbf{K}_B$, see [18], defined for a single mode as

$$\mathbf{K}_B = \begin{bmatrix} K_{11}^{(1)} & 2K_{111}^{(2)}/3 \\ 2K_{111}^{(2)}/3 & 2K_{1111}^{(3)} \end{bmatrix}. \tag{3.9}$$

and which should be positive definite. The lowest eigenvalue of $\mathbf{K}_B$ for the STEP identified models considered for Figs 3.3 and 3.4 are shown in Table 3.1. Note that two of these models (both based on 12-mode) yield non-physical negative eigenvalues. Further, there is a significant sensitivity of this lowest eigenvalue to the specific value of q_1 used. These findings confirm the difficulties involved in identifying an accurate model using the STEP procedure, Eqs (3.5)-(3.8).

The perceived weakness of this procedure is that the identification is conducted near the undeformed configuration for which the linear terms are much larger than the quadratic ones, themselves much larger than the cubic terms. That is, in conditions in which the critical balance of the terms on the left-hand-side does not take place. In this light, it was proposed to shift the baseline point around which the identification is achieved from the undeformed state to one in or near the expected difficult conditions, e.g. in a snap-through configuration of the curved beam. This baseline solution admits the representation

$$\underline{u}_0 = \sum_{n=1}^{M} q_{n,0}\ \underline{\psi}^{(n)} \tag{3.10}$$

Then, the test displacement fields imposed for identification are

$$\underline{u} = \underline{u}_0 + q_n\ \underline{\psi}^{(n)} \tag{3.11}$$

$$\underline{u} = \underline{u}_0 + q_n\ \underline{\psi}^{(n)} + q_m\ \underline{\psi}^{(m)} \quad m \geq n \tag{3.12}$$

$$\underline{u} = \underline{u}_0 + q_n\ \underline{\psi}^{(n)} + q_m\ \underline{\psi}^{(m)} + q_r\ \underline{\psi}^{(r)} \quad r \geq m \geq n \tag{3.13}$$

More specifically, for each value of n = 1, ..., M, three cases of the form of Eq. (3.11) were considered with q_n = +q, -q, and q/2 as before with q typically smaller than the thickness. The four cases corresponding to positive and negative values of q_n and q_m in Eq. (3.12) were also included for each n and $m \geq n$. Finally, all eight cases associated with positive and negative values of q_n, q_m, and q_r for $r \geq m \geq n$ and all n were used.

The displacement fields of Eqs (3.11)-(3.13) include generalized coordinates along all basis functions and thus no simplification of Eq. (3.4) takes place as in Eq. (3.6). Accordingly, the stiffness coefficients were obtained by a least squares solution of Eq. (3.4) with the complete set of displacement fields imposed by Eq. (3.11)-(3.13). Note that the linear, quadratic, and cubic stiffness coefficients are often of very different magnitudes and thus an appropriate scaling of the terms is recommended to keep low the condition number of the least squares matrix. It was also found beneficial to include the equations corresponding to two different baseline displacement fields $\underline{u}_0$.

A preliminary assessment of the above revised model identification approach was obtained by computing the modal force vs. modal displacement curves corresponding to the Nastran scaled displacement of Fig. 3.2. This effort was accomplished first in a single mode format using the two baseline solutions with modal displacements of 3.328e-4 and 1.14e-2 and q_1 = 4e-4. The corresponding curve, named “LS”, see Fig. 3.3, matches very closely its Nastran counterpart. The computation was also repeated with the 12-mode model of [11] with baseline solutions corresponding to the projection on this basis of the Nastran displacements induced by the load P = 1.7 lb/in and P = 2 lb/in. The results, named “LS”, see Fig. 3.4, again match very closely those obtained with Nastran. Finally, the eigenvalues of the matrix $\mathbf{K}_B$ were also recomputed for the two models and the results are shown in Table 3.1. Note that these values are significantly larger than those obtained with the STEP algorithm highlighting the difference in the identified models.

Chapter 4

BASIS SELECTION

4.1 Introduction

The two previous chapters have focused on the derivation of the parametric form of the reduced order model governing equations, Eqs (2.8) and (3.5), and on the estimation of the parameters from a set of well chosen finite element solutions. The last key aspect of the construction of reduced order models is the selection of the basis functions $\underline{\psi}^{(n)}$. In this regard, the expected features of the reduced order model are that (i) it leads to an accurate representation of the full finite element results and (ii) it includes a "reasonably" small number of basis functions.

The selection of such a basis is not as straightforward a task as in linear systems. Consider for example a flat homogenous structure subjected to transverse loads. In the linear response range, only transverse deflections result from the loading. However, these deflections induce a stretching in the in-plane direction and thus give rise to in-plane motions as well which are a second order effect and thus not captured by linear analyses. Nevertheless, such motions must be captured when constructing the nonlinear reduced order model.

As another example of complexity introduced by nonlinear effects, note the existence of "symmetry breaking bifurcations". The response of the symmetric curved beam shown in Fig. 4.1 to a uniform dynamic loading is known (see [4]) to be symmetric, as in the linear case, for small loading levels. However, when the response becomes large enough, antisymmetry arises through a

nonlinear coupling of antisymmetric and symmetric modes. In such cases, it is thus necessary to also include antisymmetric modes in the basis to accurately capture the beam response.

In light of the above observations, this chapter is focused on the clarification of the steps followed for the selection of the basis used in connection with the curved beam of Fig. 3.1.

4.2 Representation Error

Since the selection of the basis is not a straightforward task, it is necessary to quantify the appropriateness of a particular choice of modes for the representation of the response. It is proposed here to introduce the representation error

$$\mathrm{E_{rep}} = \frac{\left\| \underline{u} - \underline{u}_{proj} \right\|}{\left\| \underline{u} \right\|} \tag{4.1}$$

where $\underline{u}$ is a particular response of the finite element model (referred to as a test case) and $\underline{u}_{proj}$ is its projection on the basis selected, i.e.

$$\underline{u}_{proj} = \sum_{n=1}^{M} q_{n,proj}\, \underline{\psi}^{(n)} \tag{4.2}$$

where

$$q_{n,proj} = \underline{\psi}^{(n)T} M_{FE}\, \underline{u} \tag{4.3}$$

assuming that the basis functions $\underline{\psi}^{(n)}$ are orthonormalized with respect to the finite element mass matrix M_{FE}.

A basis will be considered to be acceptable for the modeling of the structural response when the representation error for a series of test cases, including both static and dynamic ones, is below a certain threshold. Visual correlations of the responses $\underline{u}$ and their projections suggest that this threshold should be taken of the order of 0.01.

Note that even a zero representation error does not guarantee that the reduced order model constructed with the basis will lead to a good match of the ROM and finite element predicted displacement fields as the generalized coordinates $q_n(t)$ will not be obtained from Eq. (4.3) but rather through the governing equations, Eqs (2.8) and (3.5). So, the representation error should be considered as only an *indicator*, not an absolute measure of the appropriateness of the basis. Further, the worth of the representation error is dependent on the test cases selected which must span the space of loading and responses of interest. For example, including only symmetric basis functions and considering test cases in which this symmetry also holds may suggest that the basis is appropriate while in fact it may not if symmetry breaking does take place for some loadings of interest.

4.3 Dual Modes

The discussion of section 4.1 highlights that the basis appropriate for a nonlinear geometric ROM must include other modes than those considered for a linear modal model but provides no guidance on how to select them. This issue has been investigated recently, see [8], and it has been suggested that the "linear basis", i.e. the modes necessary in linear cases, be complemented by "dual modes" which capture the nonlinear interactions in the structure.

While the construction of the dual modes is applicable to any structural modeling, it is most easily described in the context of an isotropic flat structure, e.g. beam or plate, subjected to a transverse loading. Selecting an appropriate basis for the transverse displacements follows the same steps as in a linear analysis in which no further modeling is necessary. When the response level is large enough for nonlinear geometric effects to be significant, small in-plane displacements appear in the full solution which are associated with the "membrane stretching" effect. While small, these in-plane motions induce a significant softening of the stiffening nonlinearity associated with pure transverse motions.

One approach to construct a full basis, i.e. modeling both transverse and in-plane displacements, appropriate for the modeling of the nonlinear response is to focus specifically on capturing the membrane stretching effects. The key idea in this approach is thus to subject the structure to a series of "representative" static loadings, determine the corresponding *nonlinear* displacement fields, and extract from them additional basis functions, referred to as the "dual modes" that will be appended to the linear basis, i.e. the modes that would be used in the linear case.

In this regard, note that the membrane stretching effect is induced by the nonlinear interaction of the transverse and in-plane displacements, not by an external loading. Thus, the dual modes can be viewed as associated (the adjective "companion" would have been a better description than "dual") with the transverse displacements described by the linear basis. The representative static loadings should then be selected to excite primarily the linear basis functions and,

in fact, in the absence of geometric nonlinearity (i.e. for a linear analysis) should only excite these “modes”. This situation occurs when the applied load vectors on the structural finite element model are of the form

$$\underline{F}^{(m)} = \sum_i \alpha_i^{(m)} \, K_{FE}^{(1)} \, \underline{\psi}^{(i)} \tag{4.4}$$

where $\alpha_i^{(m)}$ are coefficients to be chosen with m denoting the load case number. A detailed discussion of the linear combinations to be used is presented in [8] but, in all validations carried out, it has been sufficient to consider the cases

$$\underline{F}_i^{(m)} = \alpha_i^{(m)} \, K_{FE}^{(1)} \, \underline{\psi}^{(i)} \quad i = \text{dominant mode} \tag{4.5}$$

$$\underline{F}_{ij}^{(m)} = \frac{\alpha_i^{(m)}}{2} \left[K_{FE}^{(1)} \, \underline{\psi}^{(i)} \, K_{FE}^{(1)} \, \underline{\psi}^{(j)} \right] \tag{4.6}$$

$$i = \text{dominant mode}, \; j \neq i$$

where a “dominant” mode is loosely defined as one providing a large component of the response. The ensemble of loading cases considered is formed by selecting several values of $\alpha_i^{(m)}$ for each dominant mode in Eq. (4.2) and also for each mode $j \neq i$ in Eq. (4.3). Note further that both positive and negative values of $\alpha_i^{(m)}$ are suggested and that their magnitudes should be such that the corresponding displacement fields $\underline{u}_i^{(m)}$ and $\underline{u}_{ij}^{(m)}$ range from near linear cases to some exhibiting a strong nonlinearity.

The next step of the basis construction is the extraction of the nonlinear effects in the obtained displacement fields which is achieved by removing from

the displacements fields their projections on the linear basis, i.e. by forming the vectors

$$\underline{v}_i^{(m)} = \underline{u}_i^{(m)} - \sum_s \left\lfloor \underline{\psi}_s^T \, M_{FE} \, \underline{u}_i^{(m)} \right\rfloor \underline{\psi}_s \tag{4.7}$$

$$\underline{v}_{ij}^{(m)} = \underline{u}_{ij}^{(m)} - \sum_s \left\lfloor \underline{\psi}_s^T \, M_{FE} \, \underline{u}_{ij}^{(m)} \right\rfloor \underline{\psi}_s \tag{4.8}$$

assuming that the finite element mass matrix serves for the orthonormalization of the basis functions $\underline{\psi}^{(n)}$ (including the linear basis functions and any dual mode already selected).

A proper orthogonal decomposition (POD) of each set of "nonlinear responses" $\underline{v}_i^{(m)}$ and $\underline{v}_{ij}^{(m)}$ is then sequentially carried out to extract the dominant features of these responses which are then selected as dual modes. The POD eigenvectors $\underline{\phi}_r$ selected as dual modes should not only be associated with a large eigenvalue but should also induce a large strain energy, as measured by $\underline{\phi}_r^T \, K_{FE}^{(1)} \, \underline{\phi}_r$, since the membrane stretching that the dual modes are expected to model is a stiff deformation mode.

To exemplify the above process, a flat aluminum beam (see [17] for details), cantilevered on both ends was considered and the duals corresponding to the first four symmetric transverse modes are shown in Fig. 4.2. Note that these duals are all antisymmetric as expected from the symmetry of the transverse motions assumed. To obtain a better sense of the appropriateness of these functions, a POD analysis of an ensemble of nonlinear responses was carried out

and also shown on Fig. 4.2 are the mass normalized POD eigenvectors found for the in-plane displacements. In fact, two such analyses were conducted, one using a series of static responses and the other using snapshots obtained during a dynamic run. It is seen from these results that the dual modes proposed in [8] are in fact very close to the POD eigenvectors obtained from both static and dynamic snapshots. Note that both POD eigenvectors and dual modes are dependent on the responses, e.g. their magnitude, from which they are derived. The results of Fig. 4.2 were obtained with responses ranging typically from 0.08 to 0.8 beam thickness. In fact, in this range of displacements, the POD analysis of the static responses yielded only two eigenvectors with significant eigenvalue and thus no POD-static curve is present in Figs 4.2(c) and 4.2(d).

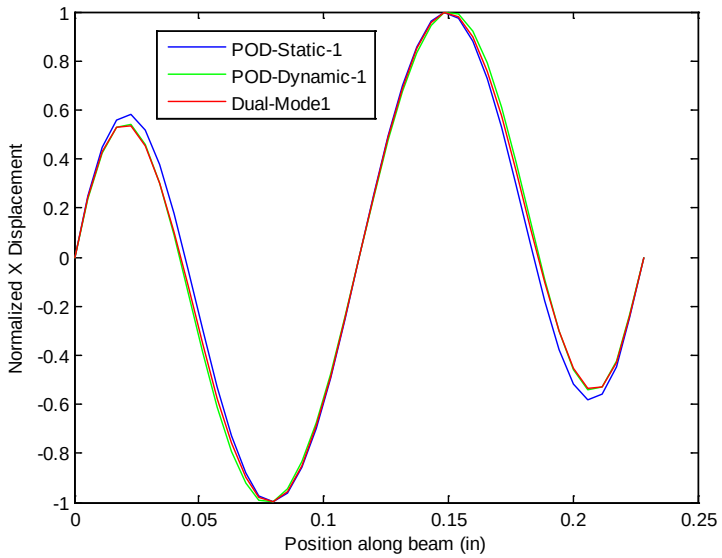
POD-Static-1
POD-Dynamic-1
Dual-Mode1
Normalized X Displacement
Position along beam (in)
1
0.8
0.6
0.4
0.2
0
-0.2
-0.4
-0.6
-0.8
-1
0
0.05
0.1
0.15
0.2
0.25

(a)

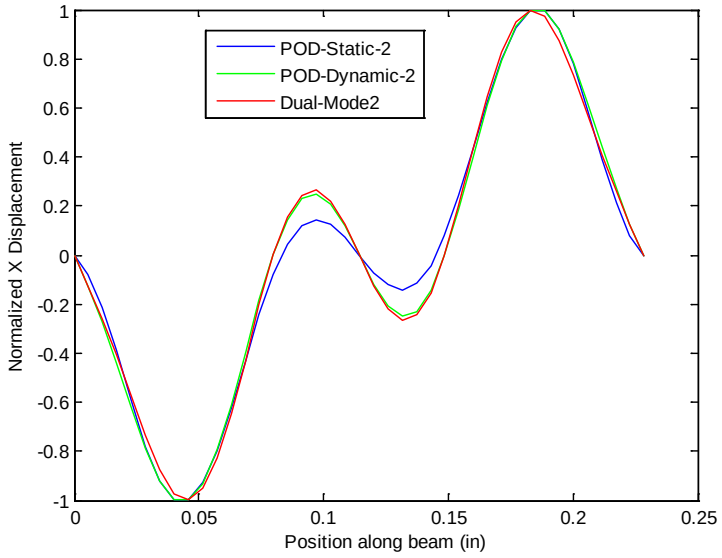
POD-Static-2
POD-Dynamic-2
Dual-Mode2
Normalized X Displacement
Position along beam (in)
1
0.8
0.6
0.4
0.2
0
-0.2
-0.4
-0.6
-0.8
-1
0
0.05
0.1
0.15
0.2
0.25

(b)

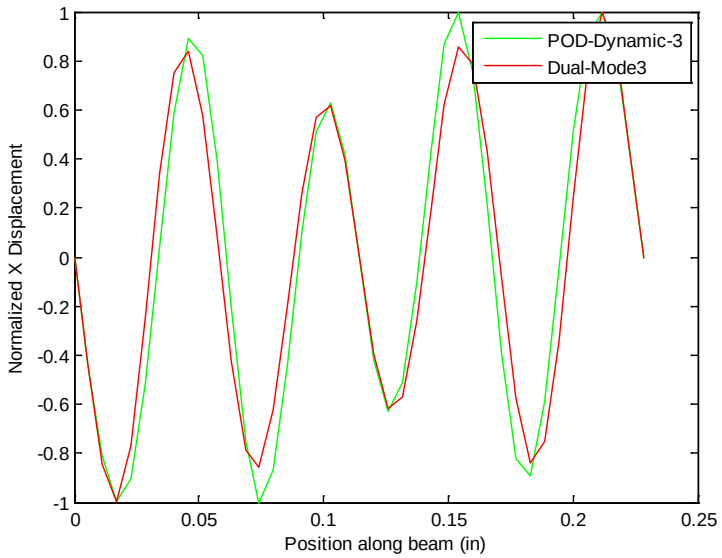

(c)

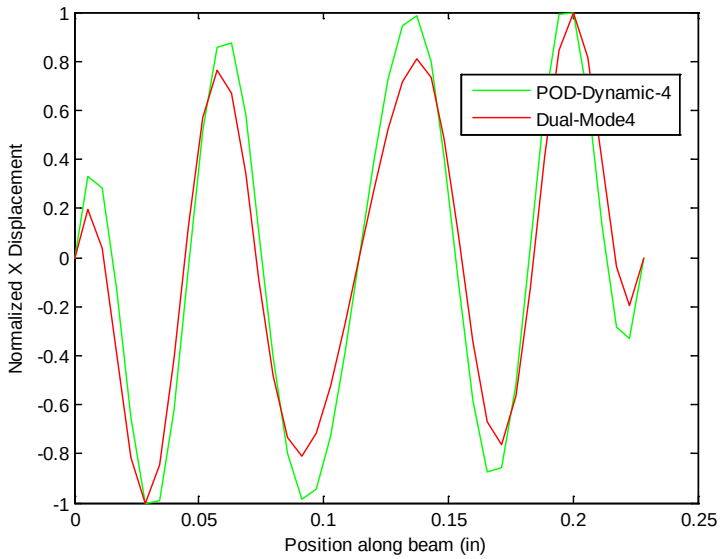

(d)

Figure 4.2. Comparison of dual modes and POD eigenvectors of static and dynamic responses, clamped-clamped flat beam.

4.4 Curved Beam - Observations

The first step in the selection of the basis for the curved beam of Fig. 4.1 was the determination of its linear mode shapes and of a series of static and dynamic nonlinear test cases to be used in the evaluation of the representation error, Eq. (4.1). Shown in Fig. 4.3 are the first 6 modes with dominant components in the plane of the beam. Modes 5 and 6 were found to be out-of-plane modes and thus were not included in the reduced order model as no such motion was observed in the validation cases considered. Displayed in Fig. 4.3 are modal displacements along the locally normal and tangential directions, not along the global X and Y coordinates.

Shown similarly in Fig. 4.4 are static responses of the curved beam induced by a uniform pressure P acting along the negative Y axis, see Fig. 4.1. For ease of presentation, the responses were scaled by their respective peak values which are given in Table 4.1. Note that the cases P = 1 and 1.5 lb/in lead to nonlinear deflections but no snap-through while the load of P = 2 lbs/in does induce such an event. Further, the normal components are all symmetric while the tangential ones are antisymmetric, consistent with the symmetry of the beam and its excitation.

Table 4.1. Maximum absolute normal and tangential displacements of some uniform negative pressure loads on the curved beam (in thickness).

	P=1	P=1.5	P=2
Max Normal Disp.	0.158	0.262	9.7

Max Tangential Disp.	0.0028	0.0046	0.2551

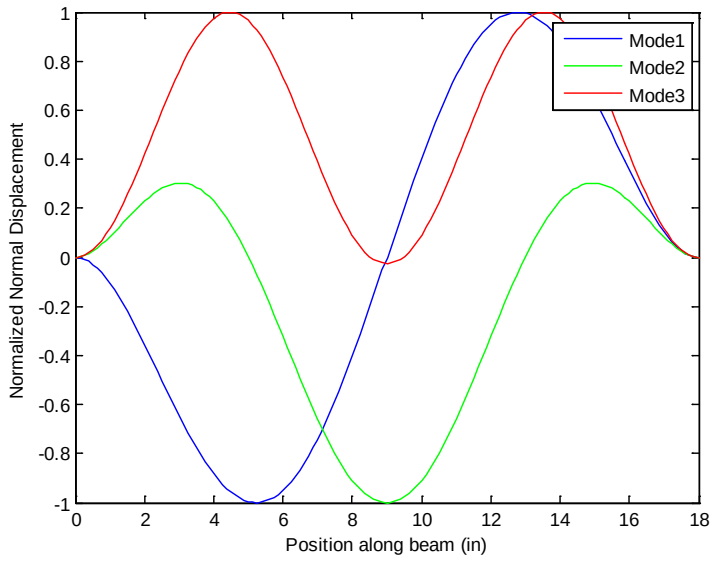

(a)

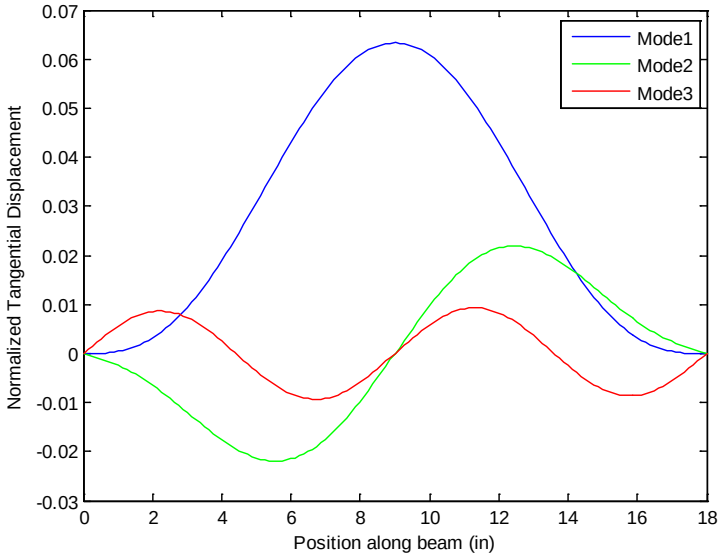

(b)

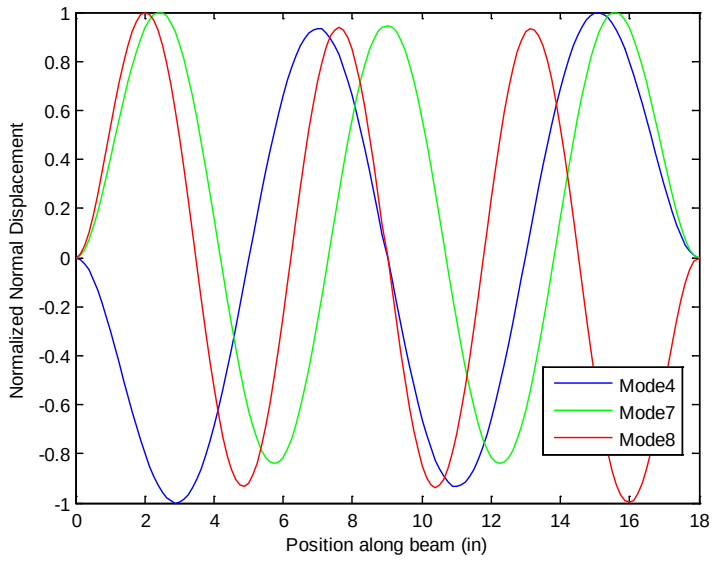

(c)

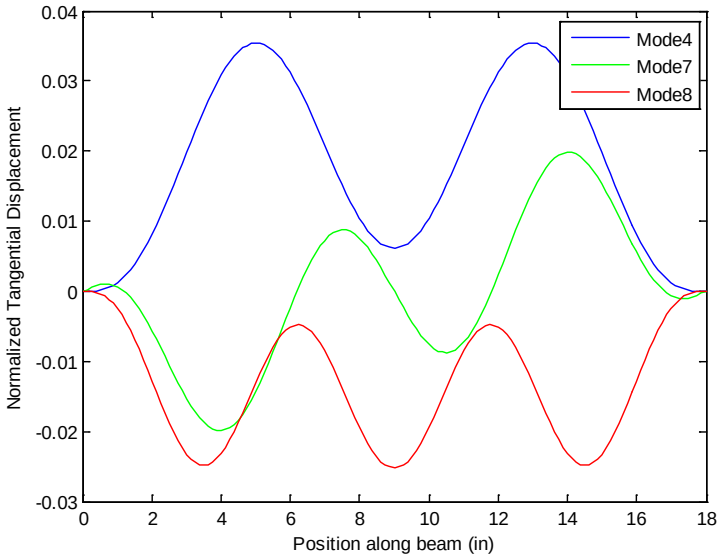

(d)

Figure 4.3. Linear mode shapes 1, 2, 3, 4, 7, and 8 of the curved beam.

(a) Modes 1, 2 and 3 – Normalized normal displacement.

(b) Modes 1, 2 and 3 – Tangential displacement.

(c) Modes 4, 7, and 8 – Normalized normal displacement.

(d) Modes 4, 7, and 8 – Tangential displacement.

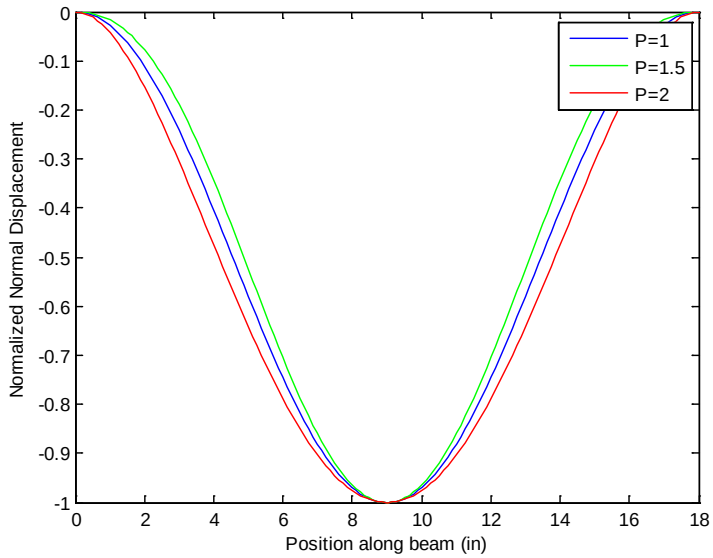

(a)

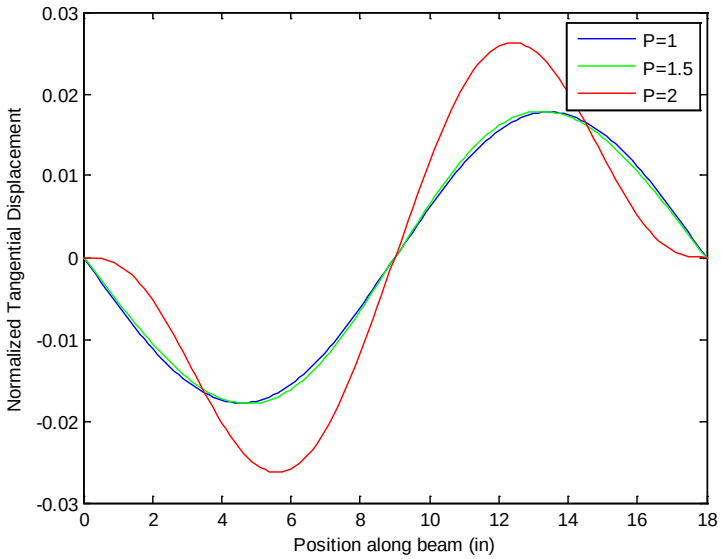

(b)

Figure 4.4. Normalized static responses of the curved beam to uniform loads *P*.

(a) Normalized normal displacement.

(b) Normalized tangential displacement.

Snap-shots of the dynamic response of the beam are shown in Figs 4.5 and 4.6. On the former figure, the responses are strongly symmetric in the normal direction and antisymmetric in the tangential, although not exactly as in the static cases, see Fig. 4.4. However, in the latter figure 4.6, no symmetry of the responses is observed, either exactly or even approximately. These observations confirm the observations of [4,11] that a symmetry breaking bifurcation takes place dynamically and thus the lack of symmetry will need to be reflected in the basis.

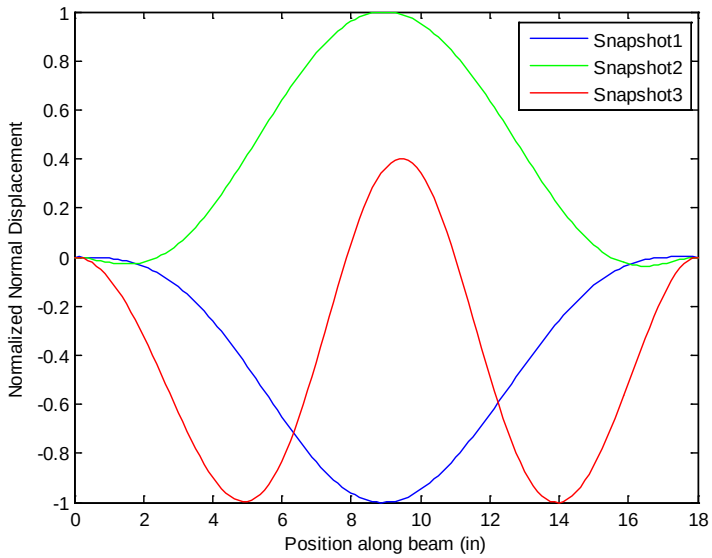

(a)

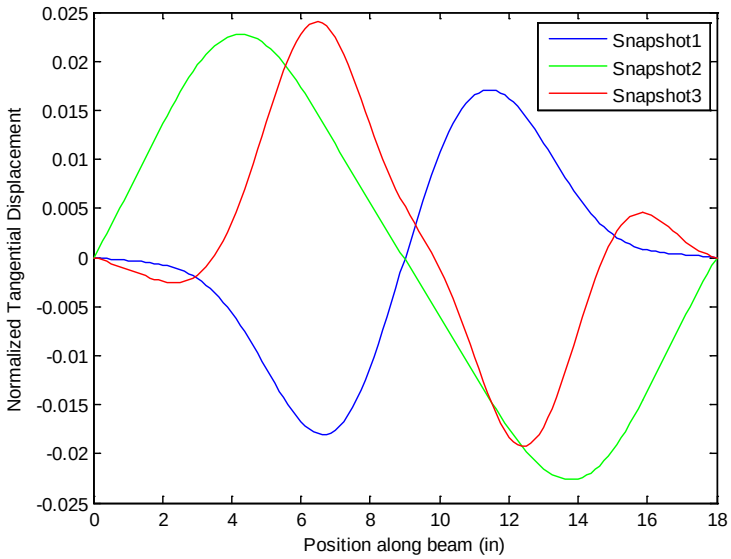

(b)

Figure 4.5. Snap-shots of the dynamic response of the curved beam - I.

(a) Normalized normal displacement.

(b) Normalized tangential displacement.

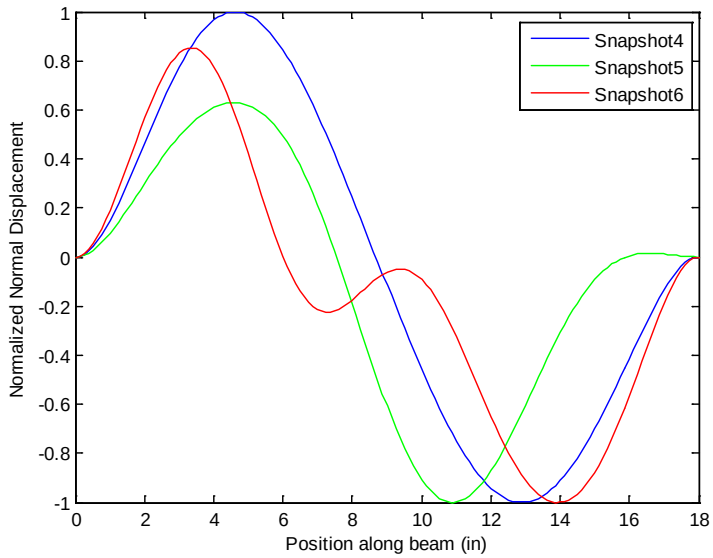

(a)

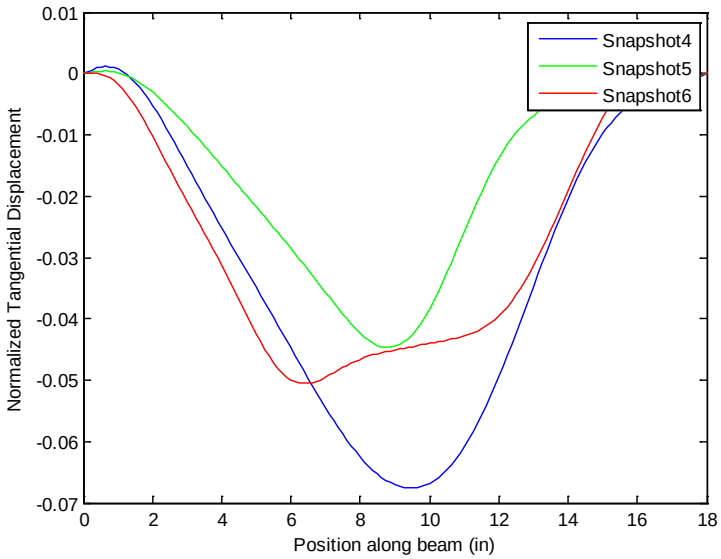

(b)

Figure 4.6. Snap-shots of the dynamic response of the curved beam - II.

(a) Normalized normal displacement.

(b) Normalized tangential displacement.

4.5 Curved Beam - Normal Basis Functions

Consistently with linear modal models, the appropriateness of the linear mode shapes to represent the nonlinear responses was first investigated. From Fig. 4.3, it is seen that all mode shapes exhibit at least one zero of the normal displacements which thus alternate (except mode 3) between positive and negative values. However, all static responses and most large dynamic ones do not, their normal displacements are all one sided and no zero at the middle (as the linear mode 3). To get an overall perspective on that issue, the ensembles of static and dynamic responses were analyzed separately in a POD format to extract the dominant features of the beam response. The corresponding POD eigenvectors of the normal components (treated separately of the tangential ones), shown in Fig 4.7, do indeed confirm the above impression: the first normal POD eigenvector of both static and dynamic responses does indeed exhibit a one-sided normal displacement reaching its maximum value at the middle, at the contrary of the linear mode shapes. However, the second normal POD eigenvector is somewhat similar to the second (lowest symmetric) mode shape. While the mode shapes are known to form a complete basis for all deflections, linear or nonlinear, of the curved beam, the above observations suggest that the convergence with the number of modes used may be slow.

On this basis, it was decided here not to use the linear mode shapes but rather a set of basis functions that is consistent with the POD eigenvectors of Fig. 4.7. Certainly, the POD eigenvectors themselves could have been selected but it was desired to select basis functions originating from a natural family of modes.

In this regard, a strong similarity was observed between the normal POD eigenvectors and the mode shapes of a flat beam spanning the same distance, see Figs 4.7. Accordingly, it was decided to use these mode shapes as basis functions for the normal direction. Note that the value of the modal displacement of the flat beam in the transverse direction was directly used for the curved beam basis functions as a normal component with zero tangential counterpart.

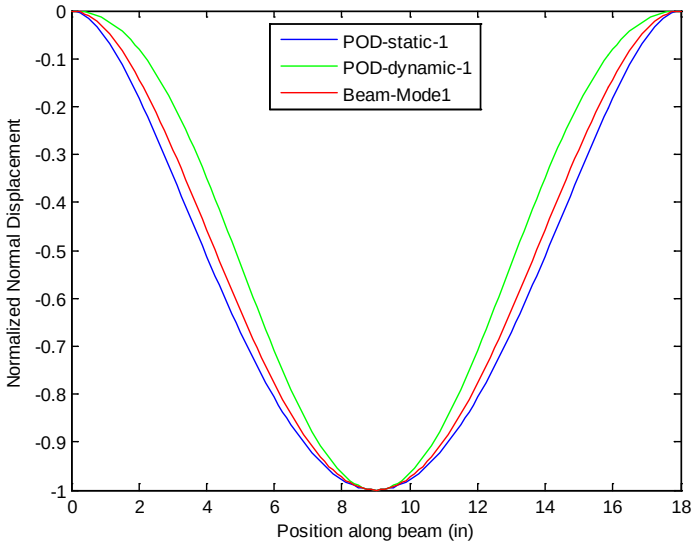

(a)

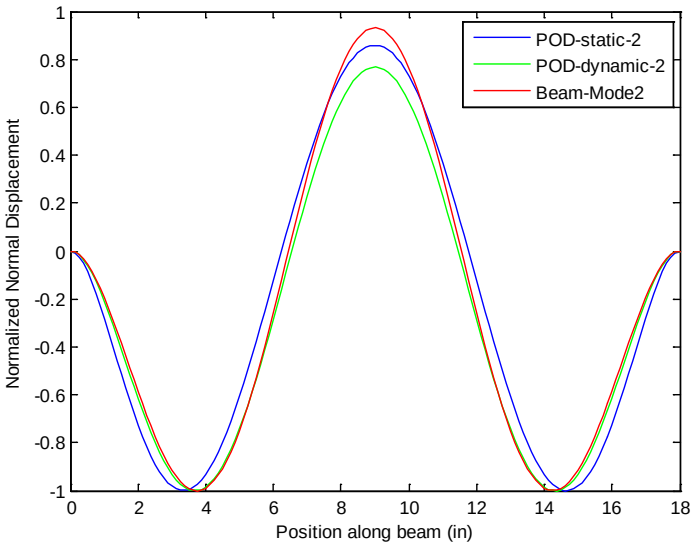

(b)

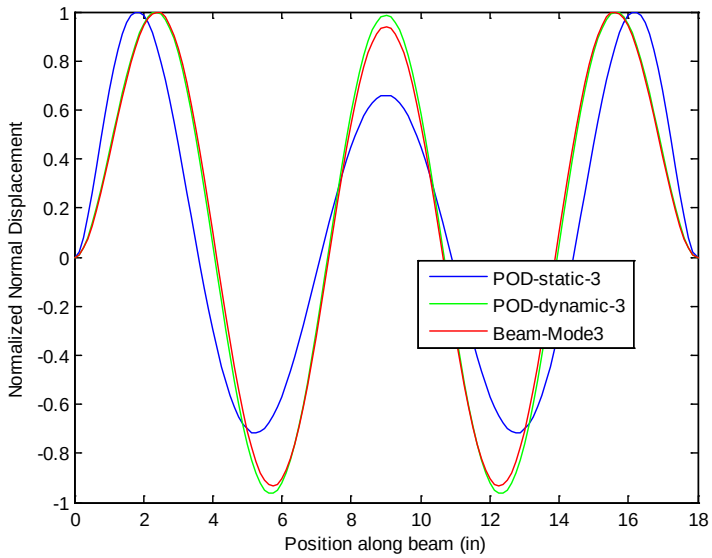

(c)

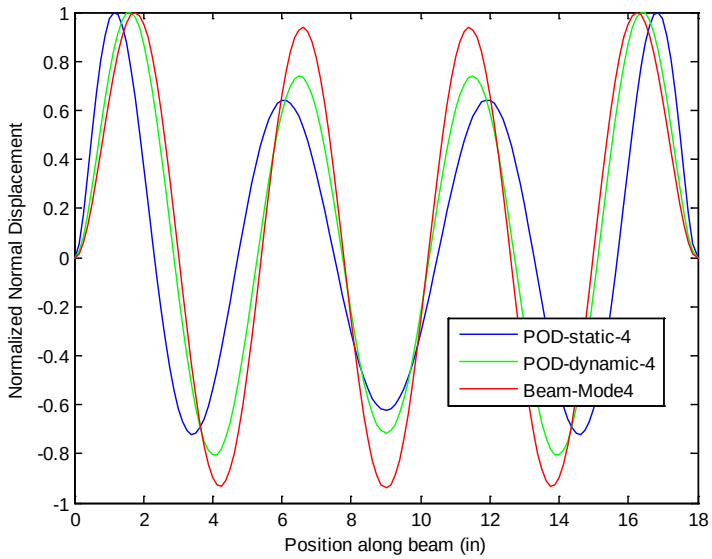

(d)

Figure 4.7. Comparison of the POD eigenvectors of static and dynamic responses in normal direction of the curved beam and the corresponding flat beam transverse modes.

4.6 Curved Beam - Tangential Basis Functions

The basis functions introduced in the previous sections do not have any tangential component and thus cannot provide a complete representation of the beam response. This situation closely parallels the flat beam where the modes first selected were purely transverse. For that structure, the "dual modes" of section 4.3 were successfully used to complement the transverse modes suggesting a similar choice for the curved beam using the normal basis functions as linear basis. In fact, the dual modes and POD eigenvectors were found to be very similar for the flat beam, see Fig. 4.2 and it was desired to first assess whether a similar property would hold for the curved beam.

Since the normal basis functions do not have any tangential component, it was decided that the dual modes that would be used should exhibit purely tangential displacements and the procedure of section 4.3 was modified accordingly by zeroing the normal components of the "nonlinear responses" $\underline{v}_i^{(m)}$ and $\underline{v}_{ij}^{(m)}$ before performing the POD analysis. The resulting dual modes corresponding to the symmetric normal basis functions are compared in Fig. 4.8 to the POD eigenvectors obtained from the ensemble of static and dynamic tangential responses. A good qualitative agreement is observed although the quantitative match is not as close as seen for the flat beam, see Fig. 4.2. On the basis of this successful comparison, the dual modes were selected to complement the normal basis functions for the representation of the curved beam response.

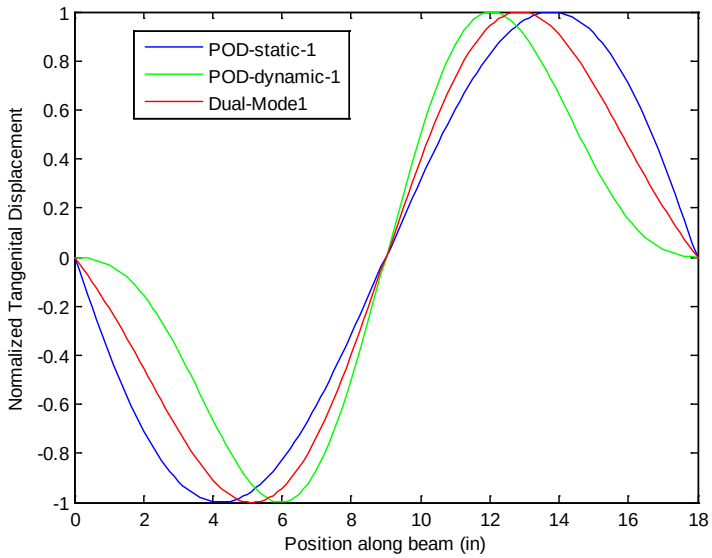
POD-static-1
POD-dynamic-1
Dual-Mode1
Normalized Tangenital Displacement
Position along beam (in)
1
0.8
0.6
0.4
0.2
0
-0.2
-0.4
-0.6
-0.8
-1
0
2
4
6
8
10
12
14
16
18

(a)

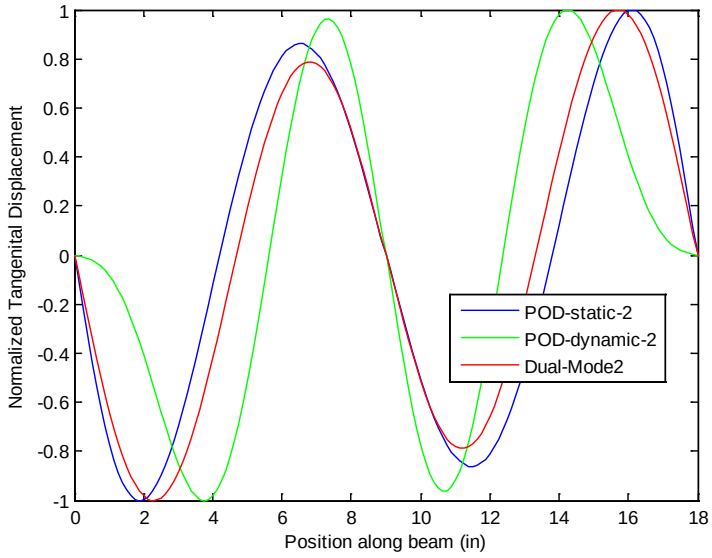
POD-static-2
POD-dynamic-2
Dual-Mode2
Normalized Tangenital Displacement
Position along beam (in)
1
0.8
0.6
0.4
0.2
0
-0.2
-0.4
-0.6
-0.8
-1
0
2
4
6
8
10
12
14
16
18

(b)

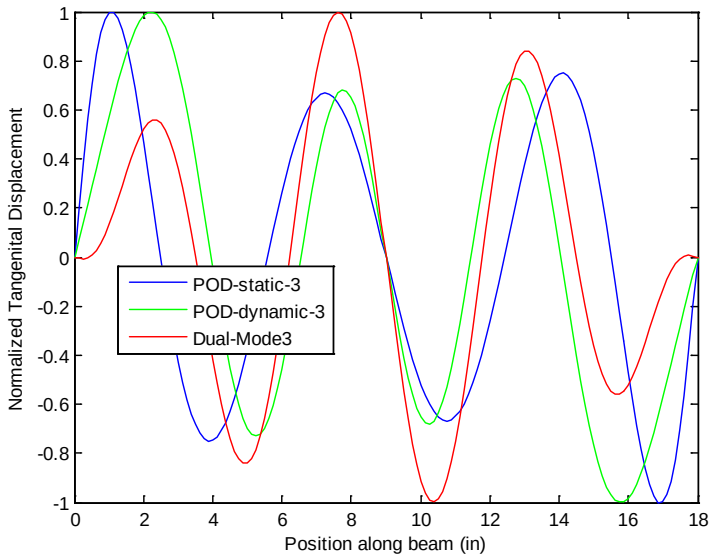

(c)

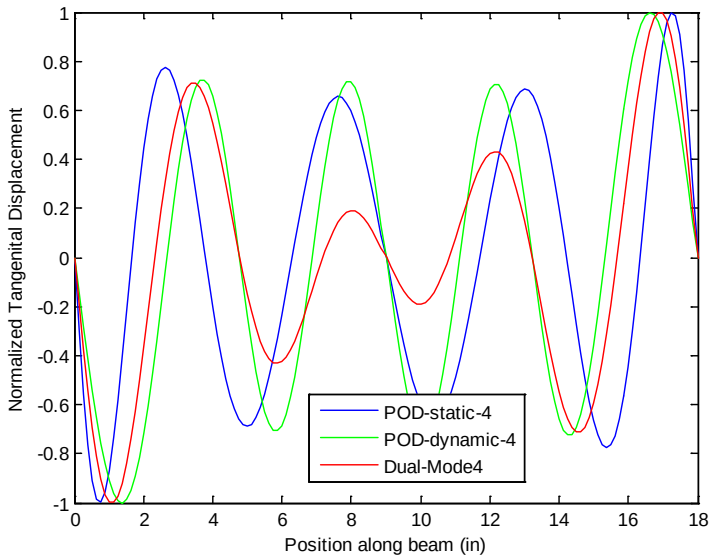

(d)

Figure 4.8. Comparison of the POD eigenvectors of static and dynamic responses in tangential direction and the dual modes, curved beam.

Chapter 5

CURVED BEAM STATIC RESPONSE VALIDATION

This chapter presents static response validation for the identification strategy based on Eqs (3.10)-(3.13) using the clamped-clamped curved beam of [4, 5, 11], see Fig. 4.1. The beam has an elastic modulus of 10.6×10^{6} psi, shear modulus of 4.0×10^{6} psi, and density of 2.588×10^{-4} lbf-sec^2/in^4. A Nastran finite element model with 144 CBEAM elements was developed to first construct the reduced order model and then assess its predictive capabilities. The reduced order model development aimed at the dynamic response to a pressure uniform in space but varying in time. This chapter focuses solely on the static response to such a loading, i.e. $F(t) = P$ constant, and shown in Fig. 5.1 is the vertical displacement induced at the middle of the beam as a function of P. Note that the beam exhibits a snap-through at P = 1.89 lb/in and that the magnitude of the snap-through deformation is quite large, of the order of 10 thicknesses. If the beam is unloaded from this point, it will not go back to the neighborhood of the undeformed position, i.e. on the left branch, until the load reduces to approximately 0.45 lb/in, which represents the snap-back condition.

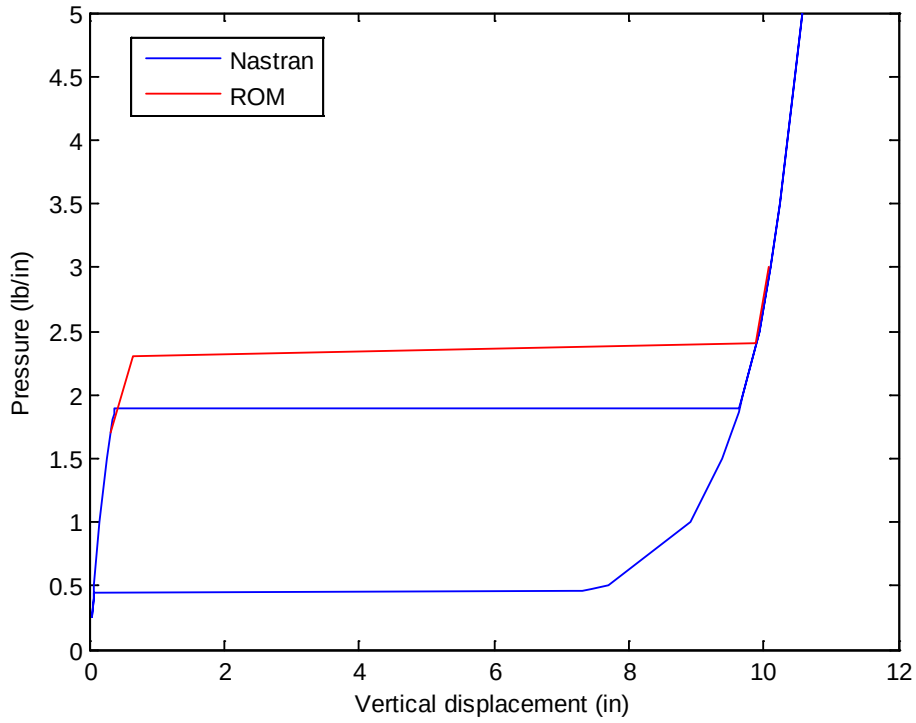

Figure 5.1. Relation between applied static pressure and vertical displacement of the beam middle, curved beam, predicted by Nastran and ROM.

The basis used for the reduced order model included the first 6 normal basis functions, see section 4.5, and the corresponding 6 dual modes with the first normal basis function dominant, see section 4.6. This process led for the present static computations to a 12-mode model similar to the one considered in [11]. To get a first perspective of how well this 12-mode basis might capture the uniform pressure static responses, the representation error was computed for a few load cases, see Table 5.1. The small magnitudes of these errors suggest that the basis is probably acceptable for the representation of the response.

Table 5.1. Representation error (in percentage) of the basis for some uniform pressure static loadings.

	P=1 lb/in	P=1.7 lb/in	P=2 lb/in	P=3 lb/in
Normal	1.095e-002	1.159e-002	1.478e-002	1.848e-002
Tangential	2.152e-002	1.637e-002	2.418e-002	4.749e-002

The construction of the reduced order model according to the STEP procedure of Eqs (3.5)-(3.8) led to the same difficulties as those encountered in [11] and described in chapter 3, i.e. difficulty in obtaining a finite valued static solution by a time marching integration of the reduced order equations of Eq. (2.8). Even when a solution could be found, it led to a poor matching of the finite element results. This issue was resolved in [11] by a detailed study of coefficients and a zeroing out of those that drove the instability; a model matching well the full finite element results was then obtained.

The present effort relied instead on the revised identification procedure, i.e. Eqs (3.10)-(3.13). Specifically, two baseline solutions were considered that correspond to the projection of the full finite element results at P = 1.7lb/in on the left branch, i.e. below the snap-through limit, and at P = 2lb/in, i.e. above the snap-through transition. No instability of the model was found in any of the computations carried out thereby suggesting that this phenomenon was indeed related to the near cancelation of terms and demonstrating the benefit of the revised identification of Eqs (3.10)-(3.13).

The assessment of the reduced model in matching the full finite element results was carried out in two phases corresponding to the two branches, left and right, of the response curve of Fig. 5.2. Shown in Fig. 5.3 are the normal and tangential displacements obtained at the load of P = 1.7lb/in which are typical of the left branch. An excellent match between Nastran and reduced order model results is obtained. A similar analysis was conducted with loading conditions on the right branch and shown in Fig. 5.4 are the normal and tangential displacements obtained for P = 3 lb/in. Both Nastran and reduced order models were then unloaded to P = 1 lb/in, see Fig. 5.5. Finally, a load of P = 10 lb/in was also considered and the responses are shown in Fig. 5.6. In all of these cases, an excellent match is obtained between the full finite element model results and the reduced order model predictions.

Even with these excellent comparisons, it should be noted that the reduced order model does not predict correctly the snap-through load. Indeed, the load-deflection corresponding to the reduced order model, also shown in Fig. 5.1, indicates that its snap-through occurs at a load of 2.3lb/in vs. the 1.89lb/in for the finite element model. Nevertheless, these overall results indicate that the identification algorithm based on Eqs (3.10)-(3.13) has led to a very reliable reduced order model.

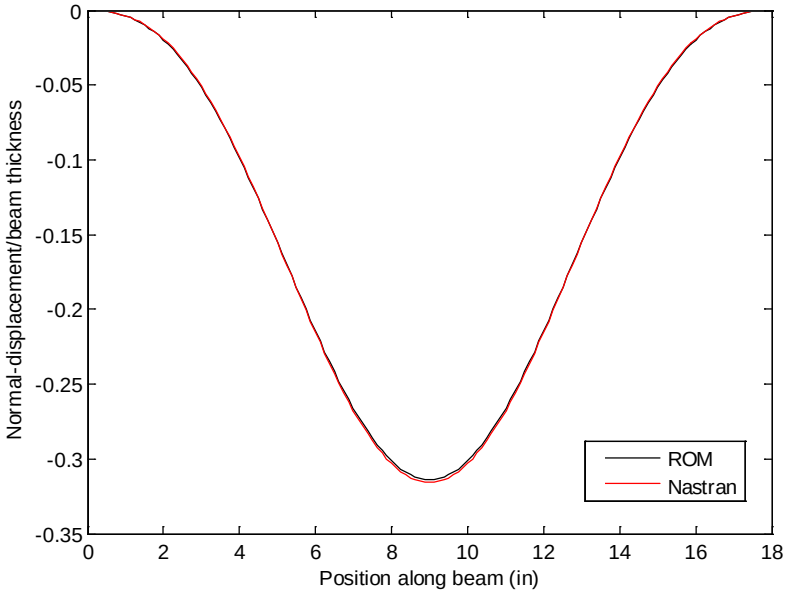

(a)

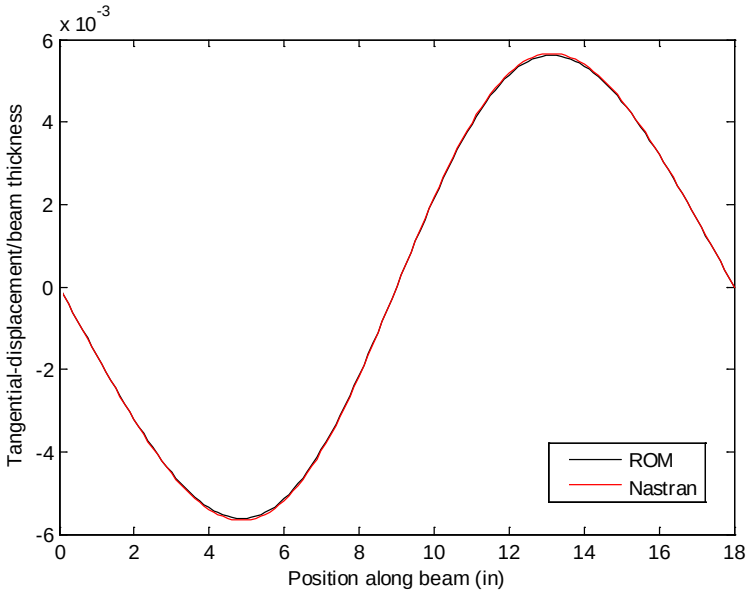

(b)

Figure 5.2. Comparison of static responses predicted by Nastran and by the reduced order model, curved beam, P = 1.7 lb/in.

(a) Normal and (b) tangential displacements.

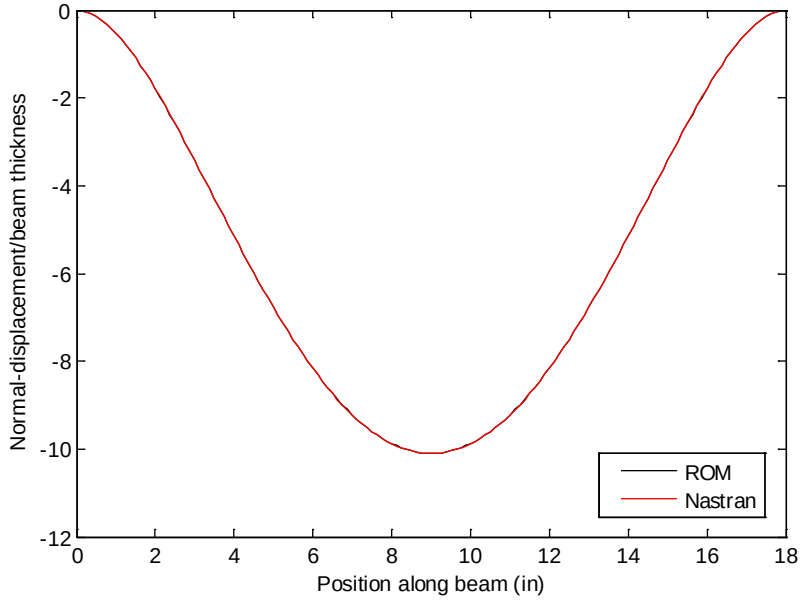

(a)

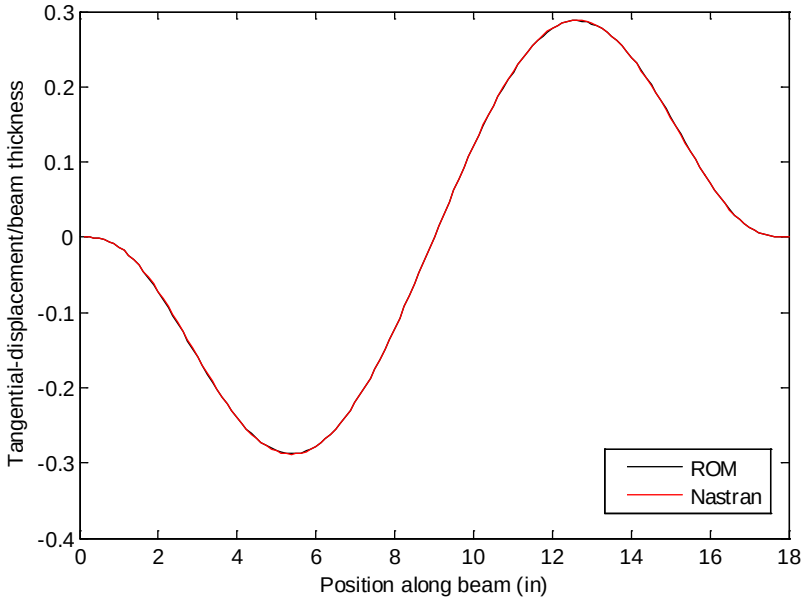

(b)

Figure 5.3. Comparison of static responses predicted by Nastran and by the reduced order model, curved beam, P = 3 lb/in.

(a) Normal and (b) tangential displacements.

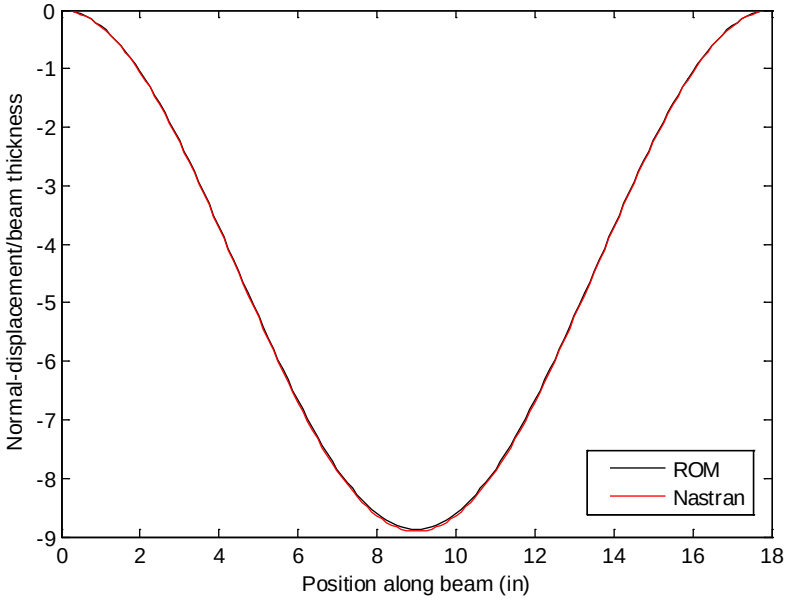

(a)

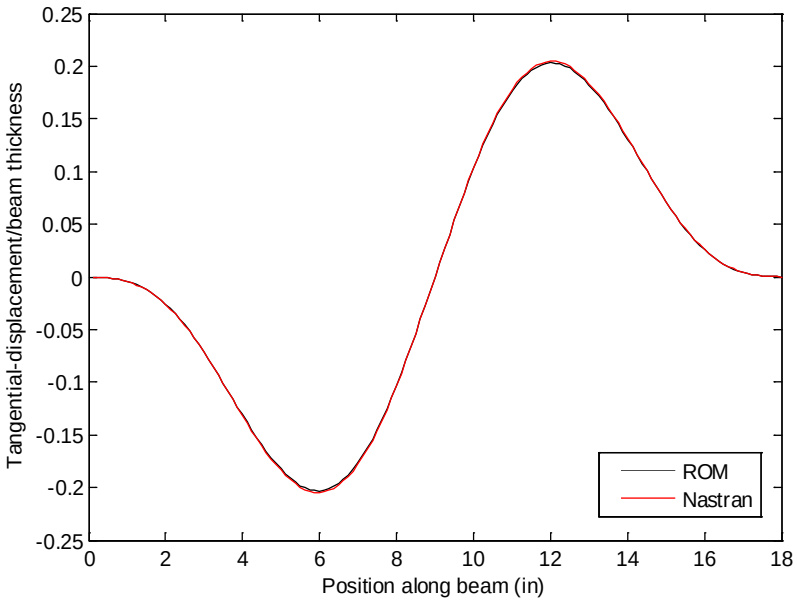

(b)

Figure 5.4. Comparison of static responses predicted by Nastran and by the reduced order model, curved beam, P = 1 lb/in (right branch).

(a) Normal and (b) tangential displacements.

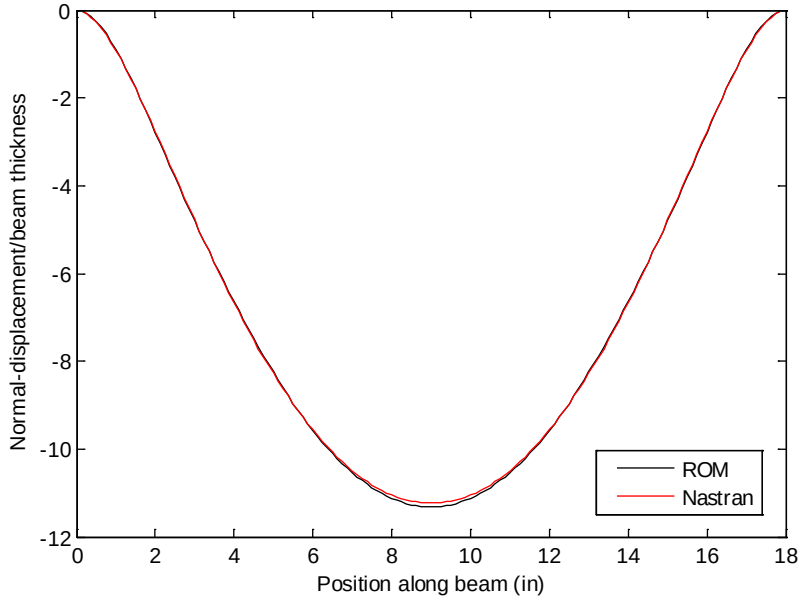

(a)

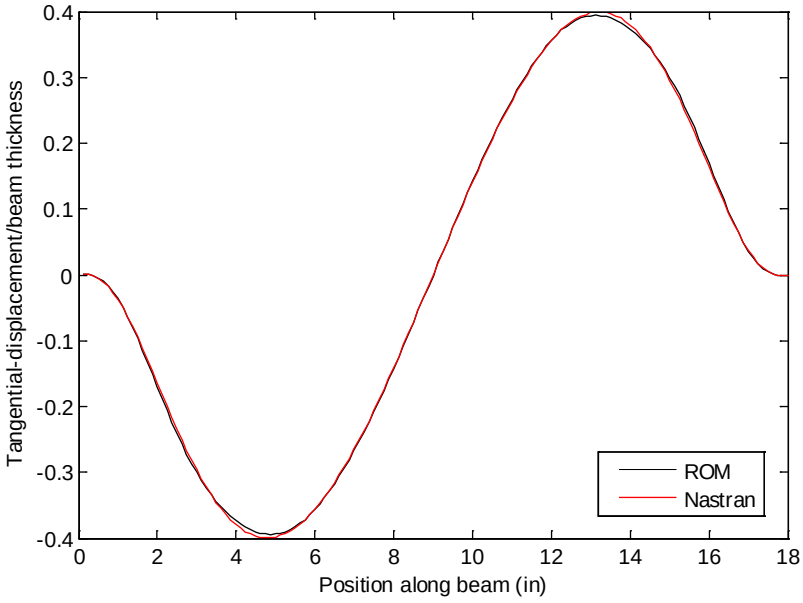

(b)

Figure 5.5. Comparison of static responses predicted by Nastran and by the reduced order model, curved beam, P = 10 lb/in.

(a) Normal and (b) tangential displacements.

Chapter 6

CURVED BEAM DYNAMIC RESPONSE VALIDATION

The 12-mode reduced order model obtained in the previous chapter only includes symmetric normal modes and thus is not appropriate for dynamic loads because of the potential occurrence of symmetry breaking. Accordingly, this chapter focuses on the construction and validation of an extended ROM that is appropriate for such dynamic loadings, i.e. includes anti-symmetric normal basis functions and corresponding dual modes.

Normal basis functions were first considered and 7 such functions were selected, more specifically 3 anti-symmetric and 4 symmetric ones, all based on the linear modes of the corresponding straight beam. Next, the 6 antisymmetric dual modes of chapter 5 were retained and complemented by 5 mostly symmetric dual modes created with the first symmetric and first antisymmetric normal basis functions as dominant. These dual modes were also made purely tangential by stripping their normal components. This process led to an 18-mode model.

Before identifying the stiffness parameters associated to this model, its adequacy to represent both static and dynamic responses of test cases was first assessed. Specifically, the representation error was computed for a series of snapshots of the dynamic response. The snapshots selected here exhibited strongly dominant symmetric or antisymmetric normal or tangential components to judge each group of the 18-mode basis separately.

Table 6.1. Representation error (in percentage) of the basis on the snapshots with symmetric normal components.

	Snap-shot1	Snap-shot2	Snap-shot3	Snap-shot4
Normal	2.46E-01	1.13E-02	4.69E-02	1.69E-01

Table 6.2. Representation error (in percentage) of the basis on the snapshots with antisymmetric tangential components.

	Snap-shot1	Snap-shot2	Snap-shot3	Snap-shot4
Tangential	2.49E-02	1.68E-02	1.38E-02	1.73E-01

Table 6.3. Representation error (in percentage) of the basis on the snapshots with antisymmetric normal components.

	Snap-shot1	Snap-shot2	Snap-shot3	Snap-shot4
Normal	1.82E-01	1.31E-01	1.37E-01	2.23E-01

Table 6.4. Representation error (in percentage) of the basis on the snapshots with symmetric tangential components.

	Snap-shot1	Snap-shot2	Snap-shot3	Snap-shot4
Tangential	1.63E-01	1.48E-01	3.39E-02	2.97E-01

The representation errors, given in Table 6.1-6.4, were found to be low enough to proceed with the identification of the stiffness parameters. Accomplishing this effort requires the selection of at least one, two were selected,

baseline solutions. To exercise all basis functions, it was desired that the baseline solutions exhibit a lack, notable preferably, of symmetry. To this end, the baseline solutions were selected as the static responses to pressure distributions linearly varying along the beam. The first such distribution varied from 0.98lb/in on the left side to 1.82 lb/in on the right one. The second varied similarly from 1.4 to 2.6 lb/in. The baseline loading P = 1.4-2.6 lb/in has a mean value of 2 lb/in and leads to a snap-through response but it is very close to symmetric. However, the baseline solution induced by the pressure P = 0.98-1.82 lb/in is not a snap-through but exhibits a significant lack of symmetry.

The dynamic validation was achieved by comparing the power spectra of the stationary responses of the center and quarter points of the beam in the global X and Y directions obtained by a full Nastran analysis and the reduced order model. The random excitation considered was uniform along the beam, in the global Y direction, and varied with time as a bandlimited white noise with a flat spectrum in the range of [0, 500Hz]. Three excitations levels were considered yielding RMS forces of 0.5, 1, and 2 lb/in, see [11]. The higher levels 1 and 2 lb/in displayed intermittent and nearly continuous snap-through excursions, respectively. The comparison of power spectra for these 3 cases and 2 locations, see Figs 6.1-6.6, demonstrates a good to very good matching, most notably at the two smallest levels, suggesting indeed the appropriateness of the reduced order model.

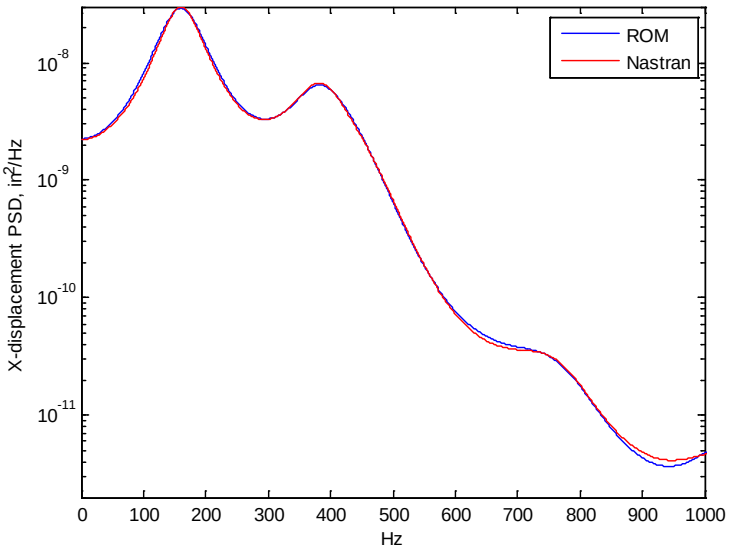

(a)

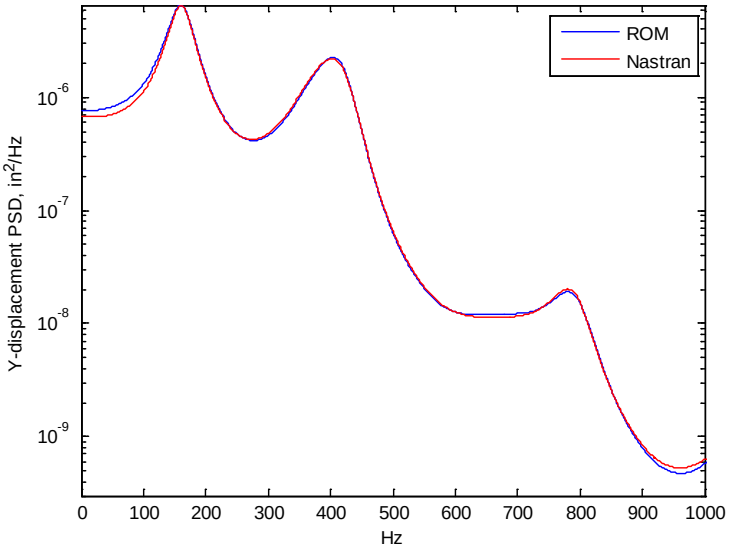

(b)

Figure 6.1. Curved beam quarter-point power spectral density for random loading of RMS of 0.5 lb/in, [0, 500Hz]. (a) *X* and (b) *Y* displacements.

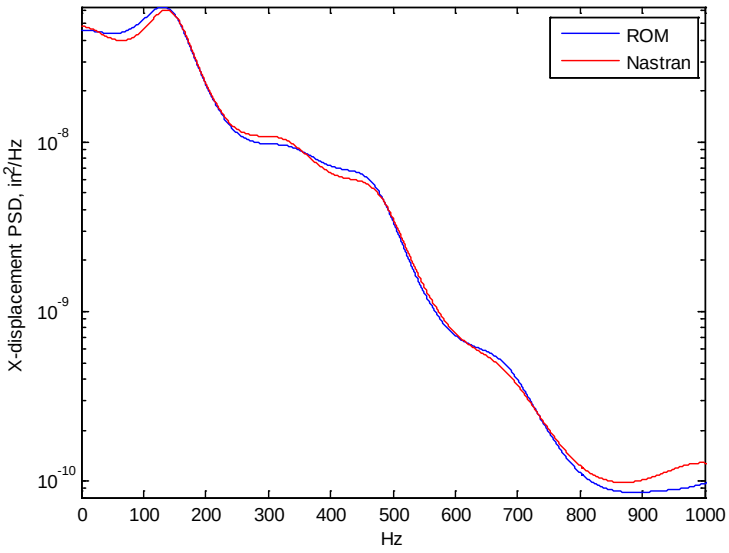

(a)

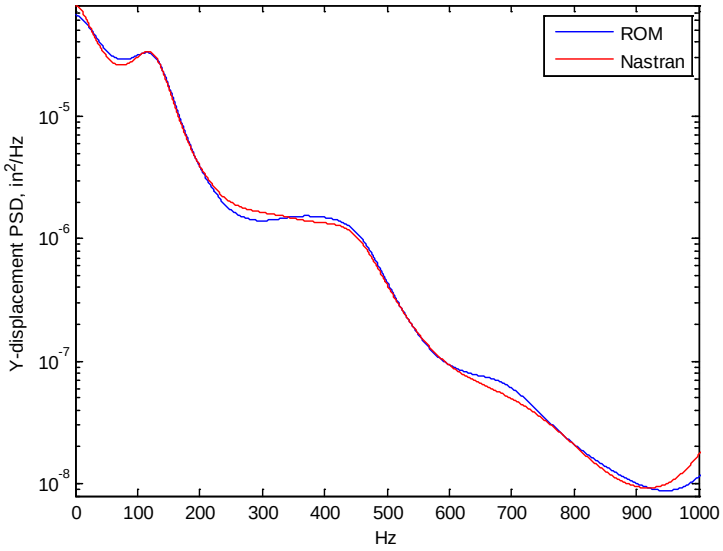

(b)

Figure 6.2. Curved beam quarter-point power spectral density for random loading of RMS of 1 lb/in, [0, 500Hz]. (a) *X* and (b) *Y* displacements.

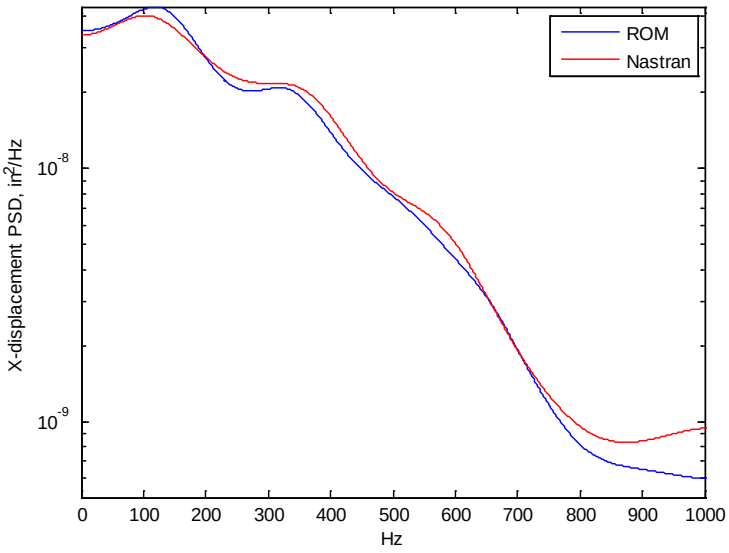

(a)

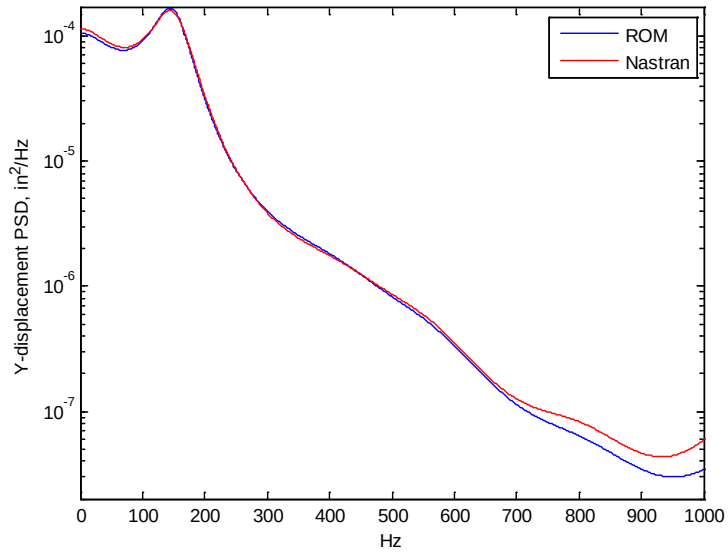

(b)

Figure 6.3. Curved beam quarter-point power spectral density for random loading of RMS of 2 lb/in, [0, 500Hz]. (a) *X* and (b) *Y* displacements.

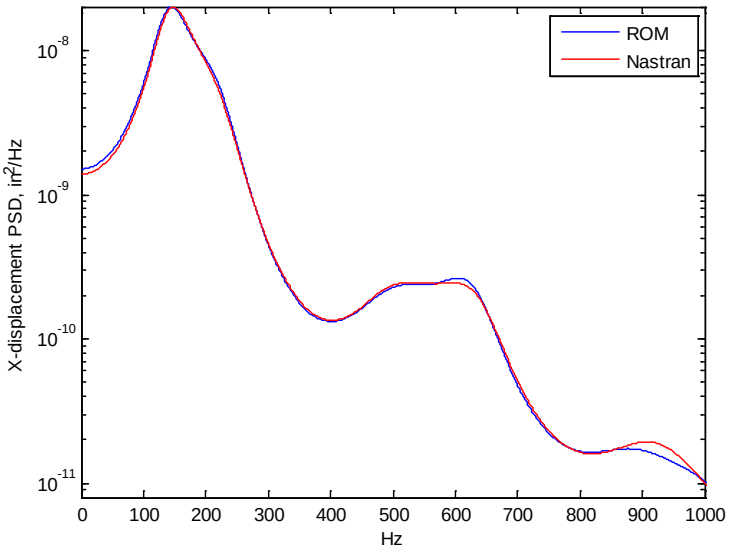

(a)

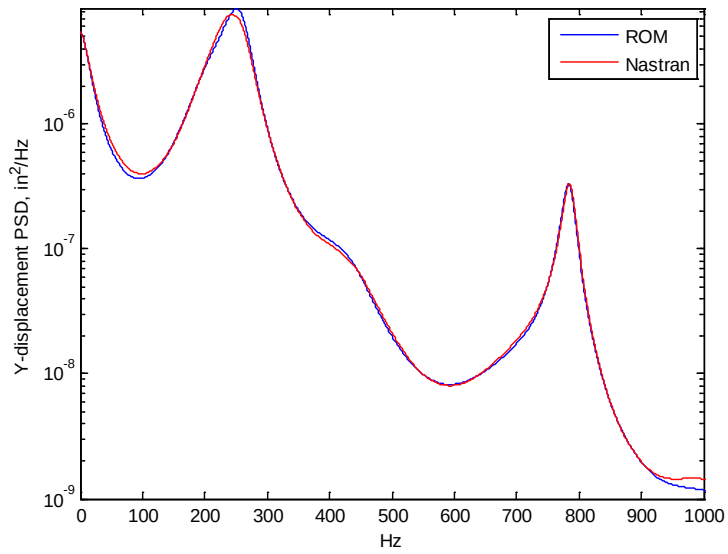

(b)

Figure 6.4. Curved beam center-point power spectral density for random loading of RMS of 0.5 lb/in, [0, 500Hz]. (a) *X* and (b) *Y* displacements.

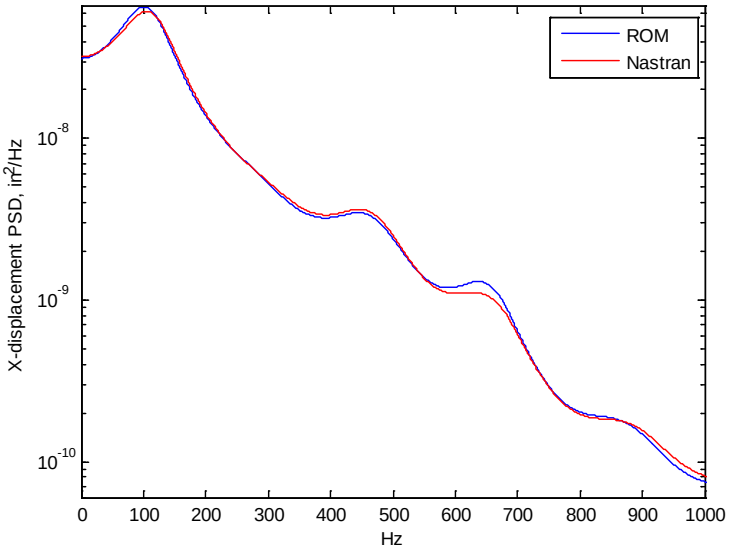

(a)

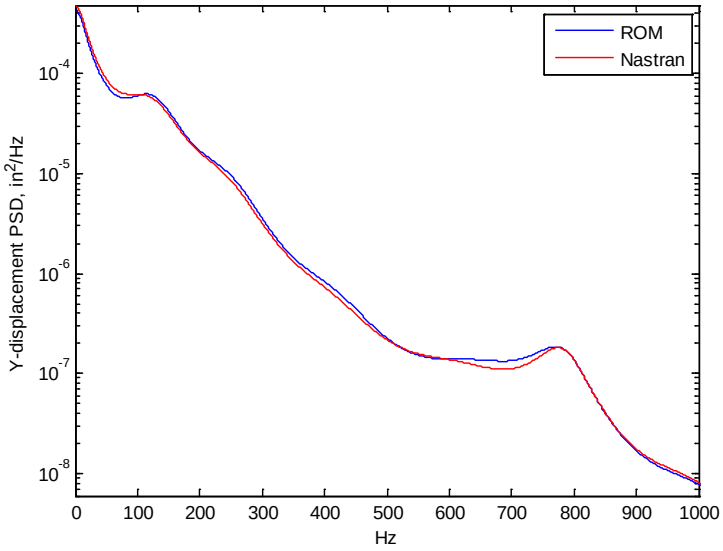

(b)

Figure 6.5. Curved beam center-point power spectral density for random loading of RMS of 1 lb/in, [0, 500Hz]. (a) *X* and (b) *Y* displacements.

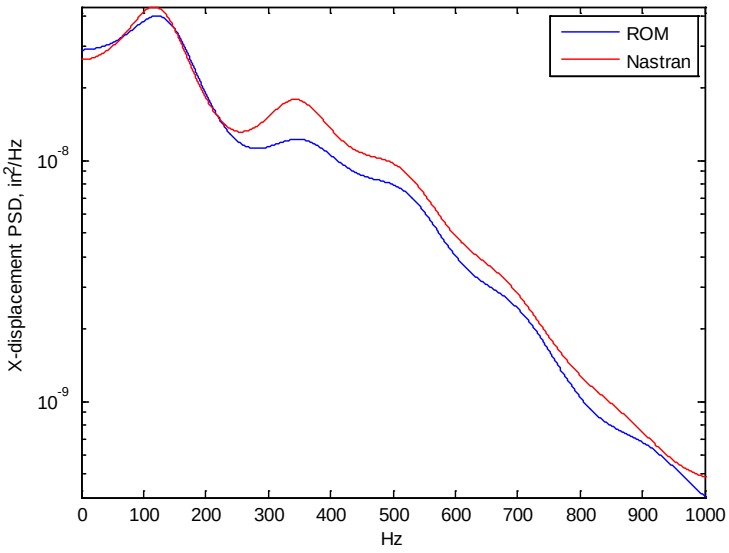

(a)

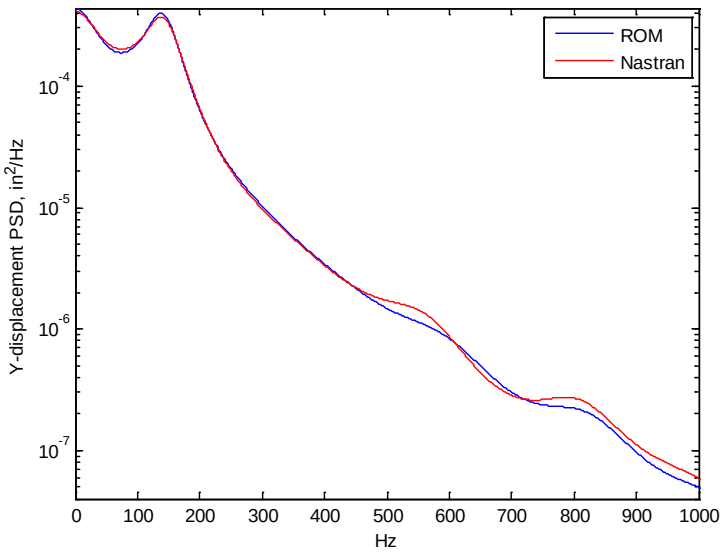

(b)

Figure 6.6. Curved beam center-point power spectral density for random loading of RMS of 2 lb/in, [0, 500Hz]. (a) *X* and (b) *Y* displacements.

Chapter 7

SUMMARY

The present investigation focused on a revisit and extension of existing approaches for the reduced order modeling of the geometrically nonlinear response of a curved beam. The work carried out addressed two particular aspects of the ROM development: the selection of the basis and the identification of the coefficients. In regards to the basis, a close relation between the recently introduced dual modes and proper orthogonal decomposition (POD) eigenvectors of the response was demonstrated for both the curved beam and its flat counterpart. This POD analysis also supported the earlier choice of normal basis functions as the linear modes of the flat beam.

In regards to the identification of the parameters, the difficulties, i.e. instability of the reduced order model, encountered in the past were first analyzed. This effort then served as the basis for the formulation of a revised identification procedure of the parameters of the reduced order model, see Eqs (3.10)-(3.13). The application of this procedure to the curved beam model removed the instability issue previously encountered and led to an excellent matching of reduced order model and finite element predictions for a broad range of external, static or dynamic, loading. Further, this matching was obtained without performing the zeroing out process suggested in an earlier investigation. The present results extend previous validation studies in demonstrating the worth of reduced order modeling of nonlinear geometric structures.

REFERENCES

[1] McEwan, M.I., Wright, J.R., Cooper, J.E., and Leung, A.Y.T, "A combined Modal/Finite Element Analysis Technique for the Dynamic Response of a Nonlinear Beam to Harmonic Excitation", *Journal of Sound and Vibration* 243 (2001): 601-624.

[2] Hollkamp, J.J., Gordon, R.W., and Spottswood, S.M, "Nonlinear Modal Models for Sonic Fatigue Response Prediction: A Comparison of Methods", *Journal of Sound and Vibration* 284 (2005): 1145-1163.

[3] Radu, A., Yang, B., Kim, K., and Mignolet, M.P, "Prediction of the Dynamic Response and Fatigue Life of Panels Subjected to Thermo-Acoustic Loading", *Proceedings of the 45th Structures, Structural Dynamics, and Materials Conference.* Palm Springs, California, 2004. AIAA Paper AIAA-2004-1557.

[4] Przekop, A. and Rizzi, S.A, "Nonlinear Reduced Order Finite Element Analysis of Structures With Shallow Curvature", *AIAA Journal* 44, no. 8 (2006): 1767-1778.

[5] Gordon, R.W. and Hollkamp, J.J, "Reduced-Order Modeling of the Random Response of Curved Beams using Implicit Condensation", *AIAA Journal* (2006).

[6] Spottswood, S.M., Hollkamp, J.J., and Eason, T.G, "On the Use of Reduced-Order Models for a Shallow Curved Beam Under Combined Loading", *Proceedings of the 49th Structures, Structural Dynamics, and Materials Conference.* Schaumburg, Illinois, 2008. AIAA Paper AIAA-2008-1873

[7] Kim, K., Khanna, V., Wang, X.Q., Mignolet, M.P, "Nonlinear Reduced Order Modeling of Flat Cantilevered Structures", *Proceeding of the 50th Structures, Structural Dynamics, and Materials Conference*. Palm Springs, 2009. AIAA Paper AIAA-2009-2492.

[8] Kim, K., Wang, X.Q., and Mignolet, M.P, "Nonlinear Reduced Order Modeling of Functionally Graded Plates", *Proceedings of the 49th Structures, Structural Dynamics, and Materials Conference.* Schaumburg, Illinois, Apr. 7-10, 2008. AIAA Paper AIAA-2007-2014

[9] Perez, R., Wang, X.Q., Mignolet, M.P, "Nonlinear reduced order models for thermoelastodynamic response of isotropic and FGM panels", *AIAA Journal* 49 (2011): 630-641.

[10] Perez, R., Wang, X.Q., Mignolet, M.P, "Reduced order modeling for the nonlinear geometric response of cracked panels", *Proceeding of the 52th*

Structures, Structural Dynamics and Materials Conference. Denver, 2011. AIAA Paper AIAA-2011-2018.

[11] Spottswood, S.M., Eason, T.G., Wang, X.Q., Mignolet, M.P, "Nonlinear reduced order modeling of curved beams: a comparison of methods", *Proceeding of the 50th Structures, Structural Dynamics, and Materials Conference*. Palm Springs, 2009. AIAA Paper AIAA-2009-2433.

[12] Rizzi, S.A. Przekop, A, "System identification-guided basis selection for reduced-order nonlinear response analysis", *Journal of Sound and Vibration* 315 (2008): 467-485.

[13] Przekop, A. Rizzi, S.A, "Nonlinear reduced-order analysis with time-varying spatial loading distributions", *Journal of Aircraft* 46 (2009): 1395-1402.

[14] Muravyov, A.A. and Rizzi, S.A, "Determination of Nonlinear Stiffness with Application to Random Vibration of Geometrically Nonlinear Structures", *Computers and Structures* 81 (2003): 1513-1523.

[15] Fung, Y.C., and Tong, P, *Classical and Computational Solid Mechanics.* River Edge, New Jersey: World Scientific, 2001.

[16] Bonet, J., and Wood, R.D., *Nonlinear Continuum Mechanics for Finite Element Analysis*, Cambridge: Cambridge University Press, 1997.

[17] Kerschen, G., Golinval, J.-C., Vakakis, A.F., Bergman, L.A., "The method of proper orthogonal decomposition for dynamical characterization and order reduction of mechanical systems: an overview", *Nonlinear Dynamics* 41 (2005): 147-169.

[18] Mignolet, M.P, Soize, C., "Stochastic reduced order models for uncertain geometrically nonlinear dynamical systems", *Computer Methods in Applied Mechanics and Engineering* 197 (2008): 3951-3963.